ORIGINAL RESEARCH ARTICLE

Preparation, Characterization, and Performance Optimization of Cu₂ZnSnS₄ (CZTS) Absorber Layer Deposited by Sol-Gel Spin Coating Technique

Sanusi Abdullahi iD, Musa Momoh iD, Abubakar Umar Moreh iD and Aliyu Muhammad Wara iD

¹Department of Physics Usmanu Danfodiyo University Sokoto, Nigeria
²Department of Science Technology, Waziri Umaru Federal Polytechnic, Kebbi State, Nigeria

ABSTRACT

This study focuses on the deposition of thin films of copper zinc tin sulphide (CZTS) on uncoated soda lime glass (SLG) substrates, followed by comprehensive characterisations using X-ray diffraction (XRD), Raman spectroscopy, and UV-V is spectroscopy. The XRD and Raman results revealed the presence of kesterite CZTS and secondary phases such as SnS (TS), ZnS, and CuSnS (CTS) of the grown thin films, providing valuable insights into the crystalline structure of the samples. UV-V is spectroscopy demonstrated that the transmittance of some of the samples exceeded 90 % in the visible region, indicating their potential for transparent and efficient electronic and optoelectronic applications. Furthermore, the effect of both thickness and annealing temperature on the optical energy gap (E_g) were studied. The allowed direct optical energy gap was found to be in the range of 2.30 to 2.94 eV for the as-deposited samples and 1.82 to 2.91 eV for the annealed samples.

INTRODUCTION

Presently, solar cells based on thin films such as Copper Indium Gallium Sulphide (CIGS) and Copper Indium Gallium (CdTe) have already achieved impressive power conversion efficiencies of about 15-20% in the laboratory (Moon et al., 2029). Unfortunately, the semiconductor materials commonly used for their production are toxic, rare, or expensive (e.g., Indium, Tellurium, etc.) (Kwak et al., 2020; Stamford and Azapagic, 2019). For the long-term viability of thin film solar cells, alternative materials are therefore needed. To compete with the above-mentioned popular materials, these materials must be relatively non-toxic, abundant, and cheap. One such material is Copper Zinc Tin Sulphide (Cu₂ZnSnS₄ or CZTS). CZTS is a quaternary structured semiconductor that is like Copper Indium Sulphide (CIS) and CIGS; the Indium in the ternary structure of CIS has been replaced with Zinc (Zn) and Tin (Sn) (Chander et al., 2024; Sadanand et al., 2020). Zn and Sn are much more abundant in the earth's crust than Indium (75 ppm for Zn and 2.2 parts per million (ppm) for Tin (Sn) compared with 0.05 ppm for Indium). CZTS is a promising thin-film material for solar cells and other optoelectronic devices (Behera and Mohan, 2019). It has gained attention due to its potential advantages over other materials, such as its abundance of constituent elements because CZTS is composed of copper, zinc, tin, and sulfur, which are relatively abundant and low-cost elements compared to

some other thin-film materials like cadmium telluride (CdTe) or copper indium gallium selenide (CIGS). Furthermore, unlike some thin-film materials containing toxic elements (e.g., cadmium in CdTe), CZTS is considered environmentally friendly, which can be advantageous for large-scale deployment and end-of-life disposal. CZTS has a tunable bandgap of 1.4 to 1.5 eV (Gezin *et al.*, 2020; Prabeesha *et al.*, 2020; Park *et al.*, 2020), which means its optical and electronic properties can be adjusted to optimize its performance for solar energy conversion applications. This material also has a high absorption coefficient ($>10^4$ cm⁻¹) for sunlight, allowing for efficient light absorption in thin layers (Hameed *et al.*, 2020; Ahmadi *et al.*, 2022; Abdullahi *et al.*, 2020; Balaji *et al.*, 2020). Therefore, only a few microns thick layer of CZTS can absorb all the photons with energies above its band gap.

It is worthy of note that to create CZTS thin films, most methods have focused on inter-diffusing and sulfidizing a stack of films that were put onto glass substrates that were either bare or Mo-coated. The mechanisms leading to the production of CZTS can be straightforward, but they can also be intricate, including a careful balancing act between inter-diffusion, evaporation, sublimation, alloying, and reaction. The formation of other phases during the process of reaching thermodynamic equilibrium and their

potential persistence as impurity phases in the film can be contingent upon the specifics of the deposition technique. It is known that several binary and ternary phases of Copper Tin Sulphides (CT/CTS) can be formed from even the most basic copper-tin combinations. These include Cu_2SnS_3, Cu_2SnS_4, Cu_4SnS_4, $Cu_2Sn_3S_7$, and $Cu_{2-x}S$. In the deposition of CZTS thin films, the existence of these phases is, therefore, expected (Ahmad *et al.,* 2021; Dong *et al.,* 2023; Olalekan *et al.,* 2021). ZTS thin films can be deposited using vacuum and non-vacuum-based techniques such as thermal evaporation (Gansukh *et al.,* 2018), RF sputtering (Behera and Mohan, 2019; Sultana *et al.,* 2022; Demir, 2021), pulsed laser deposition (Yeh, 2016), spray pyrolysis (Gadallah et al., 2018), Electrodeposition (Ahmed *et al.,* 2022), so-gel spin coating (Jagdish *et al.*; 2023; Ezealigo *et al.,* 2017; Yang *et al.,* 2022; Rabeh *et al.,* 2013) and SILAR (Sanchez, 2016). These vacuum-based techniques can deposit high-quality CZTS thin films on glass or plastic substrates but require complicated equipment to maintain vacuum and high process temperatures. Among these, the spin-coating method has the advantages of simple construction, low cost, ecological safety, and large-scale deposition of different semiconductor thin films.

In this communication, we report on the structural, optical, and electrical properties of CZTS thin films prepared by sol-gel spin coating technique on uncoated soda lime glass substrates and annealed under a Nitrogen atmosphere at 450 ^{0}C for 1 hour.

MATERIALS AND METHODS

Preparation of the sol-gel precursors

The CZTS precursor solutions for spin coating were prepared from copper (II) chloride dihydrate, zinc (II) chloride, tin (II) chloride dihydrate, and thiourea (which will act as a sulphur source) in a 2-methoxy ethanol solvent, to which monoethyl amine (MEA) was added as a dispersant to prevent the formation of precipitates. To achieve this, $CuCl_2 .2H_2O$ and $SnCl_2 2H_2O$ were first dissolved in 50 ml of 2-methoxyl ethanol at 40°C under rigorous magnetic stirring until a bluish-green solution was obtained. Next, $ZnCl_2$ was added while stirring until completely dissolved, resulting in a light-greenish-yellow solution, which indicates that $ZnCl_2$ facilitates a redox reaction between Cu^{2+} and Sn^{2+} ions. Finally, thiourea was added to prevent the possible formation of secondary phases and the loss of sulphur. The solution, after being filtered was kept in an airtight container at room temperature for 24 hours. The stoichiometric solution was prepared with a Cu: Zn: Sn: S ratio of 2:1:1:4.

Substrate cleaning

The bare soda-lime glass (SLG) substrates (25 × 10 mm) were cleaned ultrasonically in detergents (alcohol, acetone), distilled water, ethanol, and isopropanol and dried under flowing nitrogen.

Deposition of the CZTS material by sol-gel spin coating

Before spin coating, the solvent was evaporated from the precursor solutions by heating at 100°C for about 30 to 60 minutes. High spinning speeds of 1350 to 3000 revolutions per minute (rpm) were then used for about 30 seconds to ensure that the precursor fluid was spread evenly over the substrate by centrifugal force. This procedure was repeated until the desired film thickness of 450, 550, and 650nm was achieved. In all, six samples were prepared, three as-deposited samples of 450, 550, and 650nm thickness and three annealed samples also of 450, 550, and 650nm thickness.

Heat treatment (annealing)

The deposited samples of 450 nm, 550 nm, and 650 nmhick were then annealed under a nitrogen (N_2) atmosphere at a temperature of 450 ^{0}C for 1 hour and then allowed to cool at room temperature. For the annealing process, the samples were carefully inserted into a glass pipe of 2 inches in diameter and 36 inches in length in such a way as to ensure a uniform temperature distribution throughout the samples. The glass pipe was inserted into the furnace tube, which was evacuated and filled with flowing N_2 gas at a flow rate of 0.5 standard cubic centimetres per minute (sccm). After setting the annealing temperature and ramp rate, the furnace was turned on. It was heated at a maximum rate of 100 °C/s to a working temperature of 450 °C for 10 minutes. Subsequently, the furnace was switched off, and the chamber was left to cool naturally to room temperature. Once cooled, the glass tube containing the samples was carefully removed.

Characterization of the samples

To investigate the properties of the films, the following analytical techniques were employed:

Structural characterization

X-ray diffraction (XRD) patterns of the films were obtained using Xpert Pro diffractometer. The instrument operates with a Cu X-ray source, monochromatic (Kα, 1.54 Å). The samples were analysed with a glancing incident angle (θ) of 1°. The Joint Committee on Powder Diffraction Standards (JCPDS) was used to determine the crystal structure adopted. Raman spectrometry was performed using a Renishaw 1000 spectrometer using a 514 nm wavelength. The Raman system was calibrated using a silicon reference. Microstructure and the Energy-Dispersive-X-ray (EDX) of the films were examined by EVO®MA-10 scanning electron microscope at a resolution of 5000 - 10000×. Elemental compositions of the samples such as Cu/(Zn+Sn) Ratio that represents the relative abundance of copper (Cu) compared to the combined content of zinc (Zn) and tin (Sn), the Zn/Sn ratio which reflects the proportion of zinc (Zn) to tin (Sn) in the CZTS compound and metal/Sn ratio which represents the relative abundance of Cu and Zn with respect to Sn in the films were also calculated. Using the

Veeco Dektak profile meter, the thickness and surface roughness of the samples were determined.

Optical characterisation

The reflectance, absorbance, and transmittance spectra of all the samples were recorded using a UV-VIS-NIR spectrophotometer (Avaspec 2048). To cover both the visible and the infrared range of the spectrum, the wavelength region was set between 190nm to 1000nm

Electrical characterization

The grown films were also subjected to electrical characterization by the 4-point probe. The current was supplied by a Crytronics model 120 current source with a range of applied currents between 1µA to 100 mA. Voltages were measured by a Keithley model 181-nanovolt electrometer. The data obtained was used to calculate the sheet resistance and resistivity of each sample.

RESULTS AND DISCUSSION

Figures 1(a) and 1(b) illustrate the XRD patterns of the deposited thin films of CZTS on uncoated SLG substrates. In Figure 1a, the 450 nm and the 550nm samples exhibited two broad but medium intensity peaks at 2θ = 30⁰ and 43⁰, respectively. These peaks are related to CuSn (CT). Additionally, the 550nm sample shows a low-intensity peak at 2θ=28⁰, which is related to kesterite CZTS according to JCPDS card number 96-900-4751. In the 650nm sample, only peaks related to CTS at 2θ = 29⁰ and unidentified material at 2θ = 40⁰ have been observed.

In Figure 1b, it is observed that all the 3 samples display peaks related to kesterite CZTS at various diffraction angles. The 450nm sample shows peaks at 2θ=26⁰, 28⁰ 29⁰, and 32⁰. These peaks are ascribed to ZnS and CZTS as per reference codes 96-153-8616 and 96-900-4751 of the JCPDS. The 550nm sample also showed peaks related to ZnS, CZTS, and CTS indexed at reference codes 96-153-8616, 96-900-4751, and 96-152-0945 in the JCPDS. As shown in Figure 1b, the 650nm sample is composed of CZTS and its secondary phases. The peaks at 2θ=28⁰ and 47⁰ belong to kesterite CZTS, while those at 2θ=38⁰ and 43⁰ belong to CTS. Annealing under a nitrogen atmosphere has improved the crystallinity of the films, which is consistent with the average crystallite size calculated using Scherrer's equation, as listed in Table 1. It is also reported (Orletskyi et al., 2016) that an increase in the intensity of peaks of CZTS thin films may be related to the change from wurtzite to kesterite.

Calculating the size of the crystallites is done by using the Scherrer formula according to the location and the FWHM of the main diffraction peak by using Equation [1] (Sanchez et al., 2016).

$$D = \frac{K\lambda}{\beta cos\theta} \tag{1}$$

where λ (1.5406 Angstrom) is the wavelength of the X-ray and β is the full width at half maximum intensity in radians, and K= 0.9
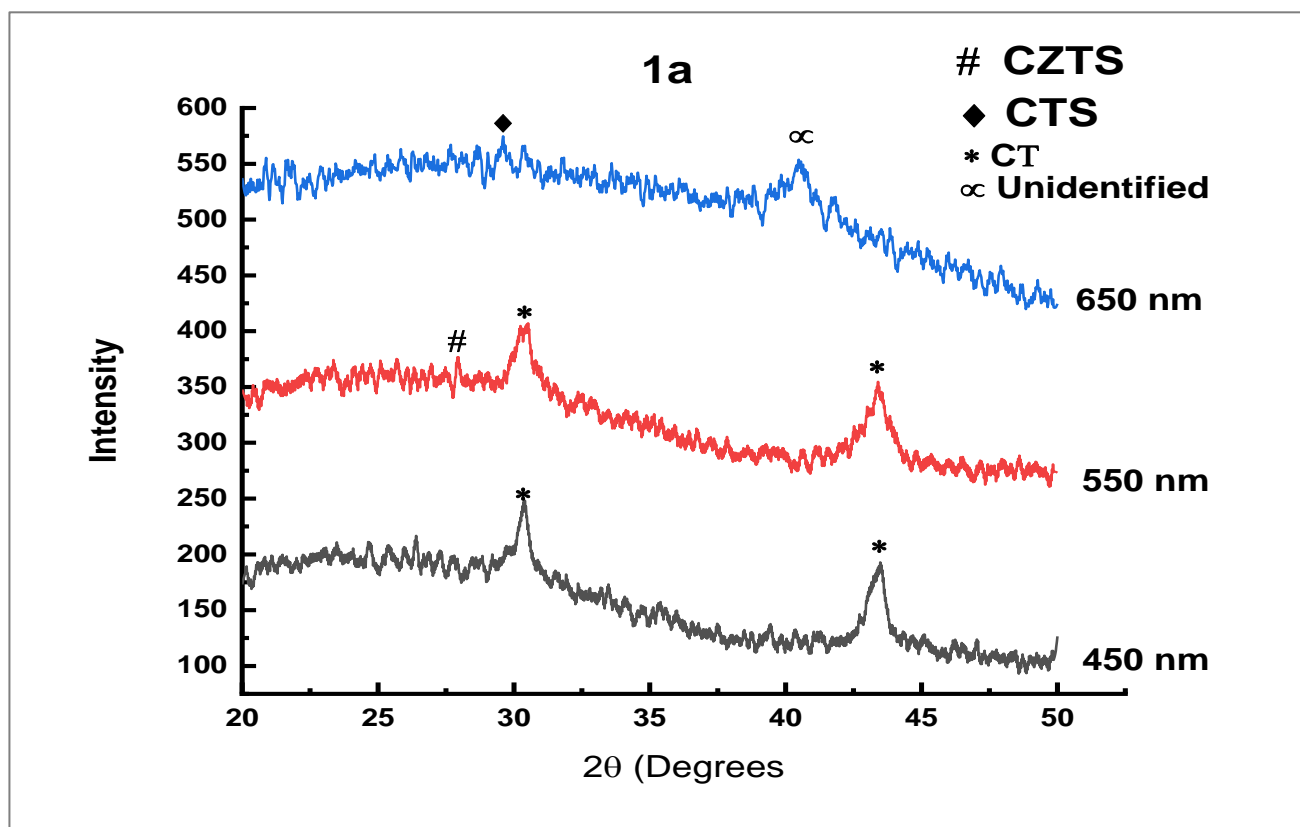
Figure 1a: XRD Pattern of as-deposited (a) and annealed
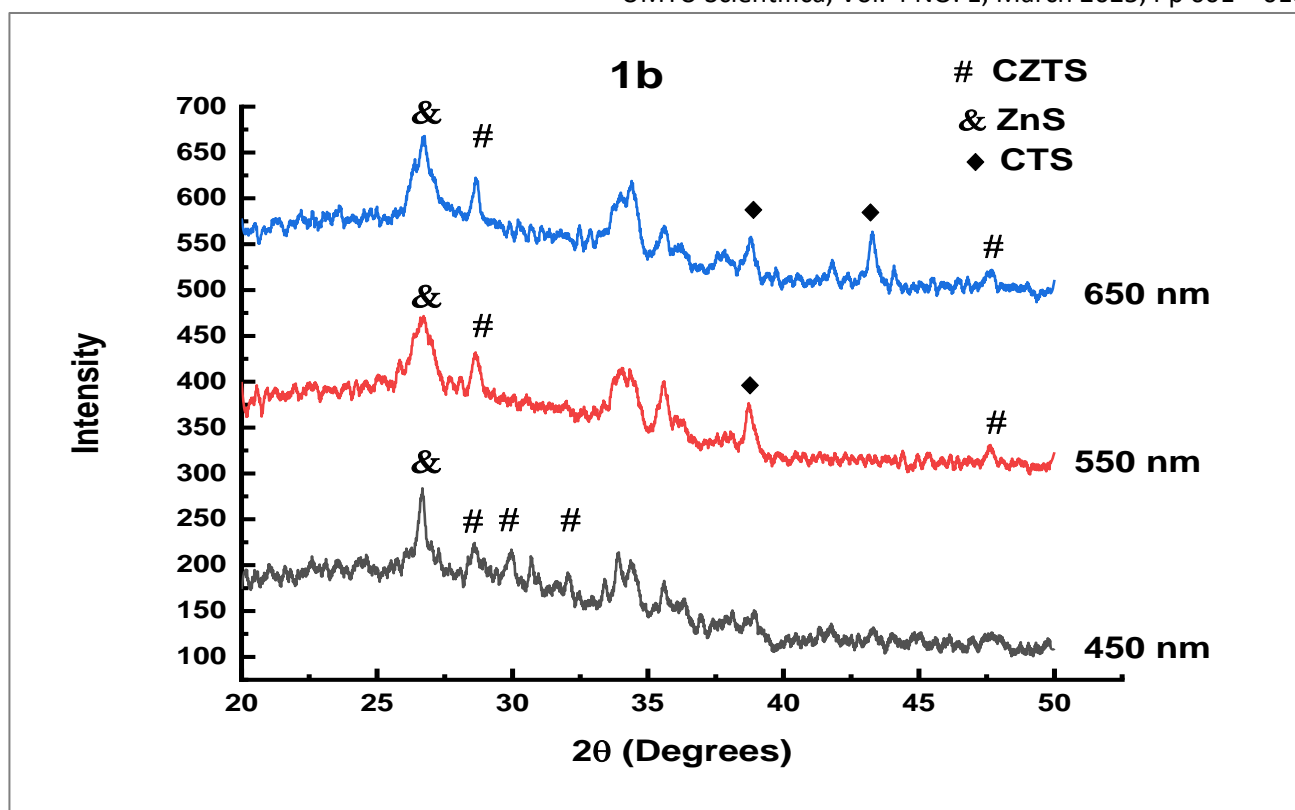
Figure 1b: XRD Pattern of as-deposited CZTS samples

Figures 2 (a) and 2 (b) display the Raman spectra of the CZTS thin films. The presence of secondary phases in the CZTS quaternary compound implies the formation of entirely different crystal structures on nanoscopic or microscopic scales. Secondary crystallites such as CTS, SnS, or even ZnS can hardly be distinguished from CZTS compounds. Although XRD is the most common tool for the determination of crystalline phases, there are situations in which diffraction peaks of different phases nearly overlap. Therefore, Raman analysis is used as a supplementary tool to distinguish and identify these phases. In Figure 2a, the as-deposited samples show not only kesterite CZTS at various wave numbers and intensities but also the expected secondary phases. The 450nm sample shows TS, CZTS, and CTS at wave numbers 215, 278, 551, and 337cm^{-1}. In this sample, the CZTS is kesterite, while the CTS is tetragonal. In the Raman spectra of the 550nm sample, Tetragonal CTS at wave number 297 cm^{-1}, TS at 315 cm^{-1}, and CZTS at 338 and 368 cm^{-1} were observed. For the 650nm sample, the peaks observed at 290, 351, and 368 belong to the monoclinic CTS and kesterite CZTS.

Figure 2b is the Raman spectra of CZTS thin films annealed under a Nitrogen atmosphere. The 450nm sample shows two peaks of kesterite CZTS at wave numbers 287 and 338 cm^{-1} and an additional peak at 352 cm^{-1} belonging to cubic ZnS. A different pattern has been observed for the 550nm sample. Apart from the kesterite,

CZTS peaks were observed at 338 cm^{-1} and 351 cm^{-1}, there also appeared a peak at 297 cm^{-1} belonging to tetragonal CTS.

The annealed sample of 650nm shows a peak at 297 cm^{-1} of tetragonal CTS and two peaks at 338 and 351 cm^{-1} referred for kesterite CZTS. It is noteworthy that the shift in Raman peaks of CZTS thin films is related to the transition from wurtzite to kesterite (Orletskyi *et al.,* 2016).

It can be seen from Table 1 that as the films get thicker, so does the lattice parameter *a* for the as-deposited samples of 450nm and 550nm thickness. The Joint Committee on Powder Diffraction Standards (JCPDS) has set a standard value of 0.5421 nm for *a*. The values obtained for the as-deposited samples are highly like those reported by (Orletskyi *et al.,* 2016) and (Barragan *et al.,* 2016). The film thickness can be the cause of the increase in parameter *a*. The lattice parameter *c* for the as-deposited samples varies along with the film thickness. According to JCPDS, the standard value of *c* for CZTS is 1.0848 nm.

Additionally, the thickness of the as-deposited samples influences the crystallite size (*D*). Among the samples, the largest crystallite size is 650 nm. The range of values obtained aligns with the parameters provided by Barragan *et al.* (2016).

In Table 1, lattice parameters *a* and *c* for the annealed samples vary with the thickness. The crystallite size increases with an increase in thickness.
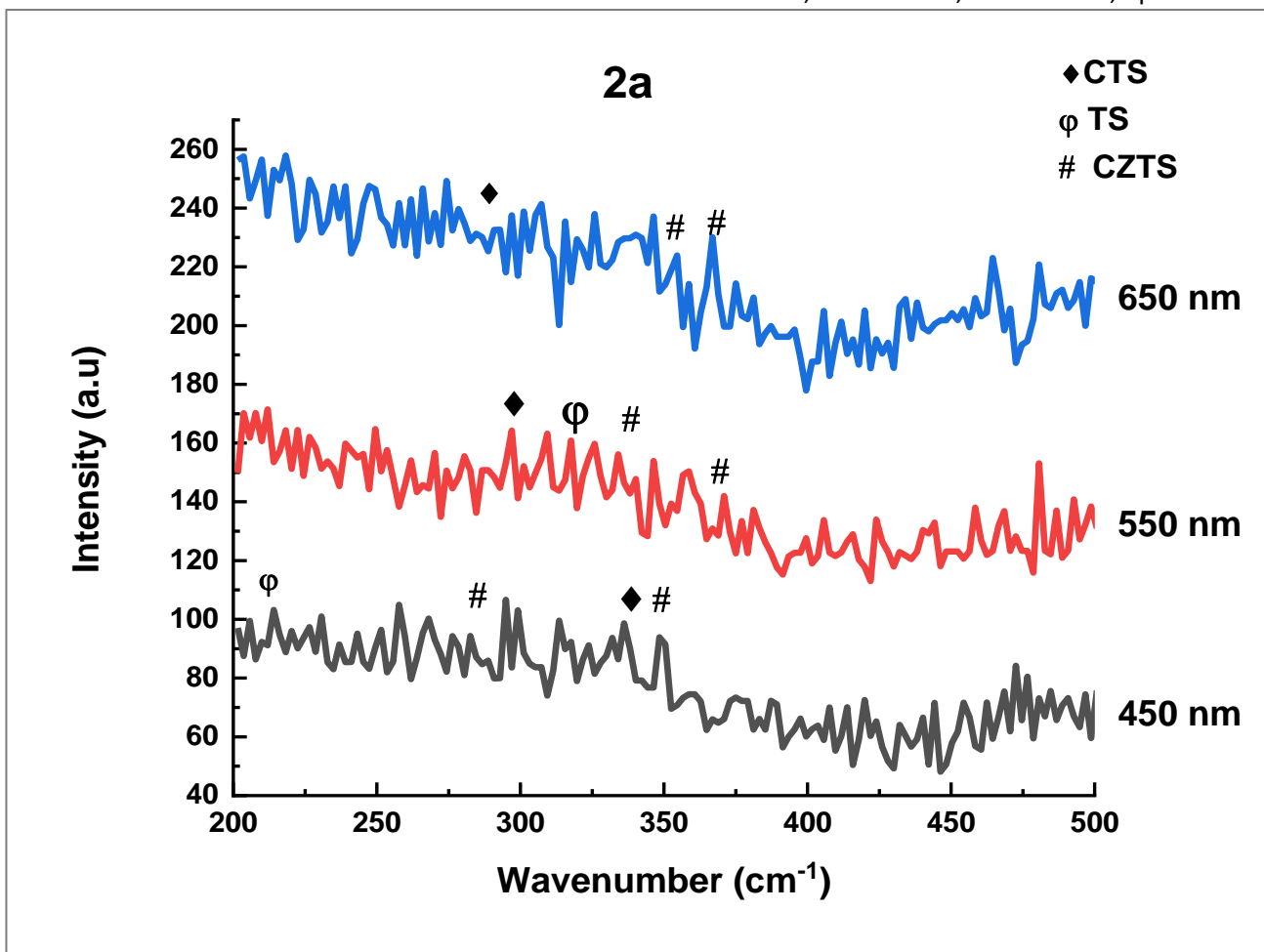
Figure 2a: Raman spectra of as-deposited and annealed
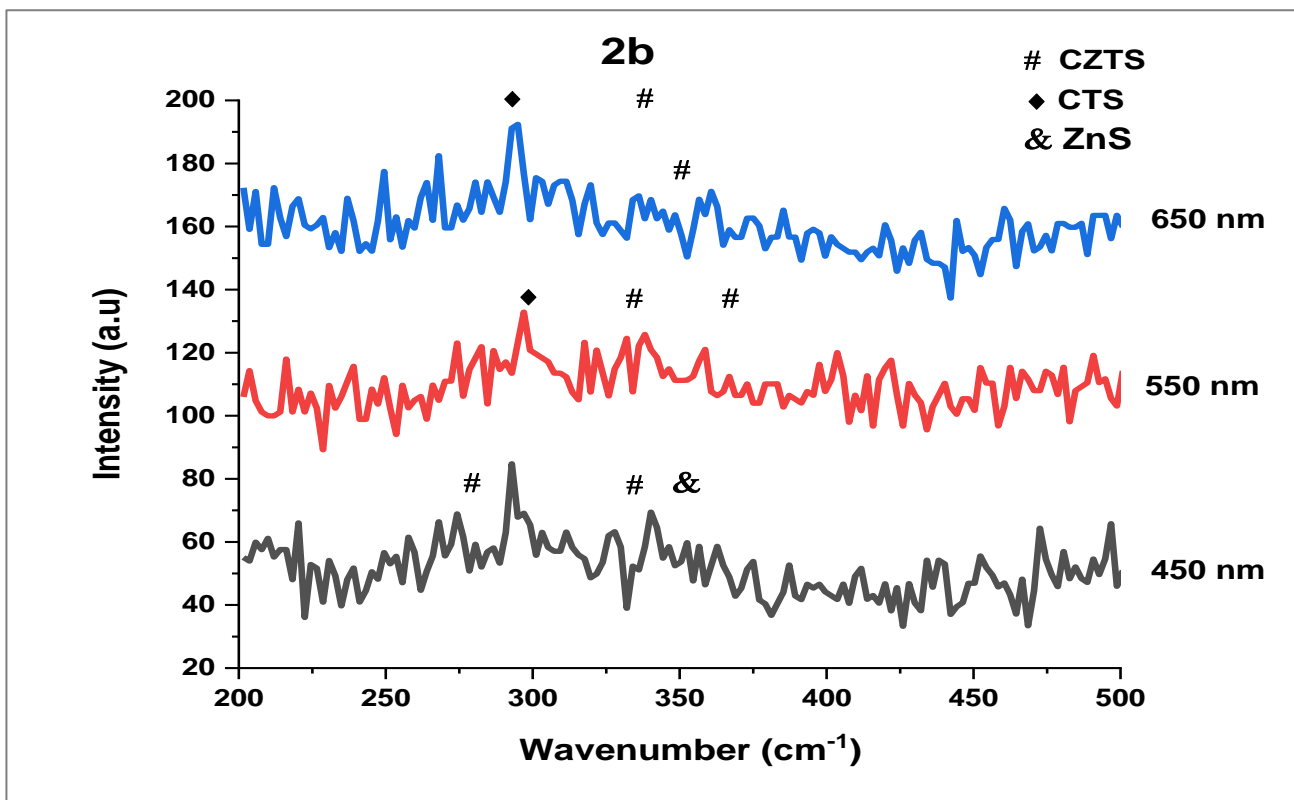
Figure 2b: Raman spectra of as-deposited CZTS samples

Table 1: Summary of some structural parameters

Sample	a (nm)	c (nm)	c/a (nm)	Crystallite size D (nm)
450nm As-dep	0.530	0.92	1.74	15.99
550nm As-dep	0.550	0.88	1.60	13.45
650nm As-dep	0.510	1.07	2.10	17.99
450nm annealed	0.600	1.09	1.82	10.58
550 nm annealed	0.530	1.06	2.00	36.70
650 nm annealed	0.542	1.08	1.99	36.70

Figures 3 (a), 3 (b), and 3 (c) display the SEM micrograph for the as-deposited samples. The SEM micrograph in Figure 3(a) reveals that the surface morphology of this film exhibits agglomerations of small grains with some voids in between. Islands and fine grains were found on the surface, and some voids were found at the glass/CZTS interface, as shown in Figure 3 (b). This is a common appearance of the CZTS thin film. In this case, a vast volume expansion during the annealing process causes a poor interface and rough surface. Additionally, uniform, homogeneous and pinhole-free grains were also observed. The morphological studies also show that the as-deposited films of 650nm thickness, or Figure 3 (c), have an absence of well-defined grains with voids.
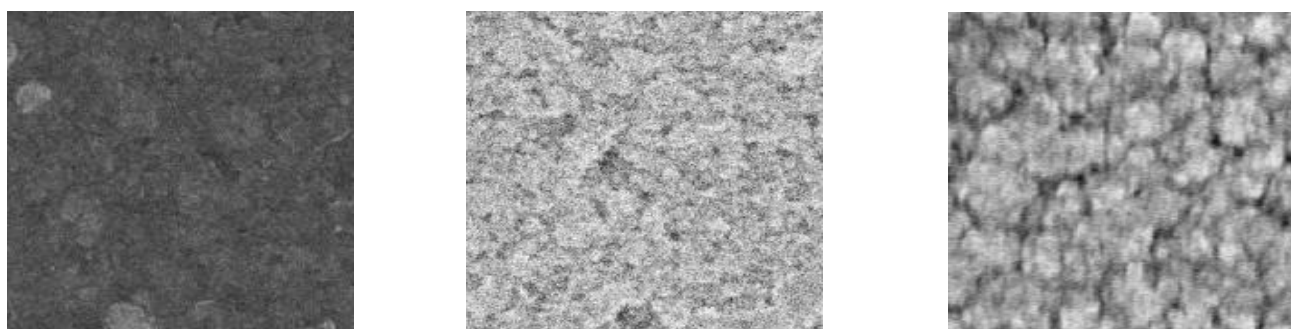
Figure 3: Morphology of the CZTS as-deposited samples of (a) 450nm, (b) 550nm and (c) 650nm

In Figure 4 (a), the film tends to grow with grains grouped in clusters of different sizes. Figure 4 (b) showed spherical grains within the diameter range of 100 nm to 300 nm and randomly oriented particle sizes were in accordance as calculated from the x-ray diffraction. The bright spots seen suggest the formation of ZnS within the sample. Large crystallites are often accompanied by the presence of secondary phases, which do not allow cells to reach high efficiency (Khushaim *et al.,* 2021). The microstructure of the annealed 650nm film is shown in Figure 4 (c) which reveals the presence of a dense surface associated with the presence of a porous structure as well as significant clear grains. There is a substantial number of voids within the sample which could be controlled by adjusting thermal treatment (Olgar *et al.,* 2020). This is most likely due to a high material loss during the annealing process (Ziti *et al.,* 2018). Furthermore, Figure 4 (c) reveals a flower-like structure, which is reported to be the consequence of annealing.
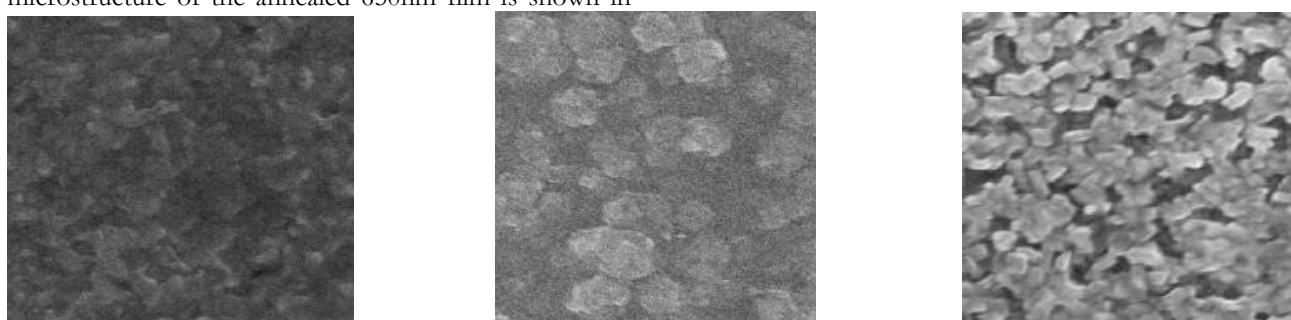
Figure 4: Morphology of the CZTS as-deposited samples of (a) 450nm, (b) 550nm and (c) 650nm

The elemental composition of the prepared films was obtained by using EDX at different zones on the surface of each sample, and the corresponding average values of the atomic percentages of Cu, Sn, S, and Zn elements are shown in Table 2. Knowing that the composition ratios of the optimized CZTS solar cell efficiency are Cu/(Zn + Sn) = 0.8 – 0.9, Zn/Sn = 1.1–1.3, and metal/S = 1.8 (Ma *et al.,* 2020). These ratios are desired for CZTS-based solar cell applications since this composition allows the formation of Cu vacancies (VCu) and antisite defects (ZnCu) in the structure and has a beneficial impact on the cell performance (Ziti *et al.,* 2018; Diwate *et al.,* 2017).

Figures 5 (a) and 5 (b) represent the optical transmittance of the CZTS thin films deposited by the spin coating method in the visible range of 250 - 850 nm. Film thickness plays an important role in the transmittance of CZTS thin films. The average transmittance (at a

wavelength of 750nm) of the 3 as-deposited samples of 450, 550, and 650nm is 7.90, 12.50, and 24.64%, respectively. This shows that transmittance increases with thickness. This pattern of transmittance increasing with thickness has also been shown by the annealed samples. The average transmittance at a wavelength of 750nm of the three as-deposited samples is 2.62%, 15.6%, and 24.04%. An increase in transmittance because of an increase in film thickness is attributed to the presence of more atoms, which make more states available for the photons to be absorbed in thicker films, as reported by (Aksoy *et al.,* 2009).

Using Tauc plots, the optical bandgap (E_g) for the as deposited and annealed CZTS thin films has been determined and shown in Figures 6 (a) and 6 (b). In the direct transition semiconductors such as CZTS, α and the optical energy band gap (E_g) are related by Equation [2] by (Salunkhe *et al.,* 2009).

$$\alpha.E \sim (hv - E_g)^{1/2} \qquad (2)$$

Where h is Planck's constant and ν is the frequency of the incident photon.

For the as-deposited samples (Figure 6a), the band gap increases with an increase in film thickness and was found in the range of 2.30 eV to 2.94 eV. In Figure 6 (b), the band gap varies with the annealing temperature. The band gaps for the annealed samples of 450, 550, and 650 nm are 2.42, 1.82, and 2.91 eV, respectively. The observed band gaps are more than or higher than the theoretical value for CZTS thin films (1.5 to 1.6 eV) (Paul *et al.,* 2024; El Mahboub *et al.,* 2024; Islam *et al.,* 2024). The higher band gap values may be due to the quantum confinement effects arising due to the nanoscale nature of the particles constituting the films (Maheshwari *et al.,* 2015). The presence of secondary phases may also be associated with the higher values of the band gap.

Several factors could be responsible for the variation in E_g following annealing. First, because of thermal expansion, electrons acquire a periodic potential; as a result, temperature affects the electronic band structure and energy gap. Second, lattice vibrations' impact on the electronic band structure and energy gap is temperature-dependent. These two variables are equally significant in determining how E_g changes during annealing. E_g renormalization could be another factor. The E_g narrowing is explained by mutual exchange, Coulomb interactions between the free electrons in the conduction band and electron impurity scattering, and the E_g renormalization model in degenerate semiconductors. This makes it easier for the conduction energy to decrease. The decrease in energy band gap because of annealing (as observed for annealed samples of 450 and 550 nm) has been reported by (Hassanien and Aki, 2019) and (El Radaf, 2020). They have attributed this phenomenon to the removal of the defect levels due to chemical compounds and thermally induced defects.

The optical reflectance for the CZTS thin films has also been analysed, as shown in Figures 7 (a) and 7 (b). Within the visible range, the as-deposited samples have shown high reflectance of the incident light. The average reflectance shown by these samples is 50.64, 56.61, and 62.90% for the 450, 550, and 650nm samples. This shows that the reflectance increases with film thickness. An average reflectance of 82.12, 78.79 and 82.58% has also been observed for the annealed samples. High reflectance is an indication that there is a high scattering of light on the samples. Another reason for the high reflectance could be the coherence between the primary light beam and the beam reflected between the film boundaries is lost and results in the disappearance of interference which in turn decreases the transmittance.

The extinction coefficient (K) shows how a material absorbs light or measures the amount of light lost due to scattering and absorption per unit volume. Change in the extinction coefficient of the samples shows that a fraction of light was lost to scattering. In Figure 8 (a), the extinction coefficient varies with thickness for the as-deposited samples. Variation in (k) has also been observed in Figure 8 (b), representing annealed samples of the CZTS thin films. This variation can also be related to the thermally induced growth of grains, which increases the packing density, as suggested by (Al-Zahraini, 2020). It has also been reported (Rahman and Khan, 2014) that small k-values in the visible and NIR regions can be attributed to higher transmission values at lower energies. This affirms that the samples are good transparent films.

Equation [3] (Islam *et al.,* 2013; Feng *et al.,* 2016) can be used to calculate the absorption coefficient. Apart from representing the probability of a photon being absorbed as it passes through a material, the absorption coefficient also expresses the strength of light absorption at a given wavelength in a material. Figures 9 (a) and 9 (b) display the absorption spectra for CZTS thin films. These Figures show results that are within the wavelength range found in the literature. As known, the valence electrons in the conduction band can only be excited by photons with energy greater than or equal to the energy band gap (E_g). In the visible wavelength region, the absorption coefficient of all the as-deposited and annealed samples of the CZTS thin films is higher or greater than $1 \times 10^{-4} cm^{-1}$. Therefore, improving energy conversion is made simpler by a direct band gap semiconductor's high absorption coefficient. Furthermore, Transitions between extended states in both valence and conduction bands may be responsible for the larger values of the absorption coefficients.

$$\alpha = \frac{1}{d} ln \left[\frac{(1-R)^2}{2T} + \left(\frac{(1-R)^4}{4T^2} + R^2 \right)^{1/2} \right] \qquad (3)$$

Where d is the film thickness.

As shown in Figures 8 and 9, the behaviour of the extinction coefficient is relatively similar to that of the absorption coefficient, where they are directly proportional to each other (k ∝ α).

Table 2: Composition ratio of CZTS samples

Sample	S (at %)	Cu (at %)	Zn (at %)	Sn (at %)	Cu/(Zn+Sn)	Zn/Sn	Metal/Sn
450nm As-dep	9.46	5.73	61.52	23.28	0.0675708	2.642612	2.88874
550nm As-dep	20.90	28.6	23.25	27.25	0.5663366	0.853211	1.90275
650nm As-dep	16.44	24.86	33.90	24.79	0.4235815	1.367487	2.37031
450nm annealed	11.77	25.52	44.07	18.63	0.4070175	2.365539	3.73537
550 nm annealed	9.53	10.59	19.50	13.70	0.3189759	1.423358	2.19635
650 nm annealed	17.20	25.66	31.52	25.62	0.4490725	1.230289	2.23185
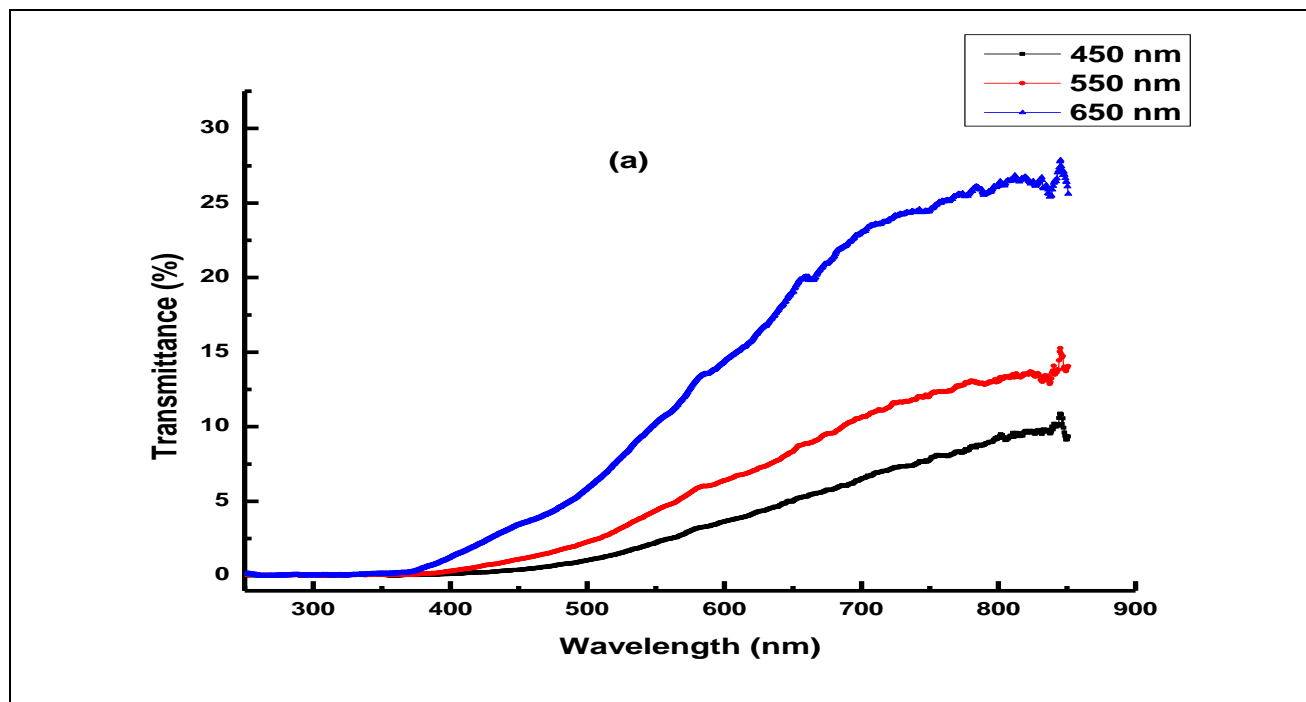
Figure 5a: Optical Transmittance of as-deposited and annealed
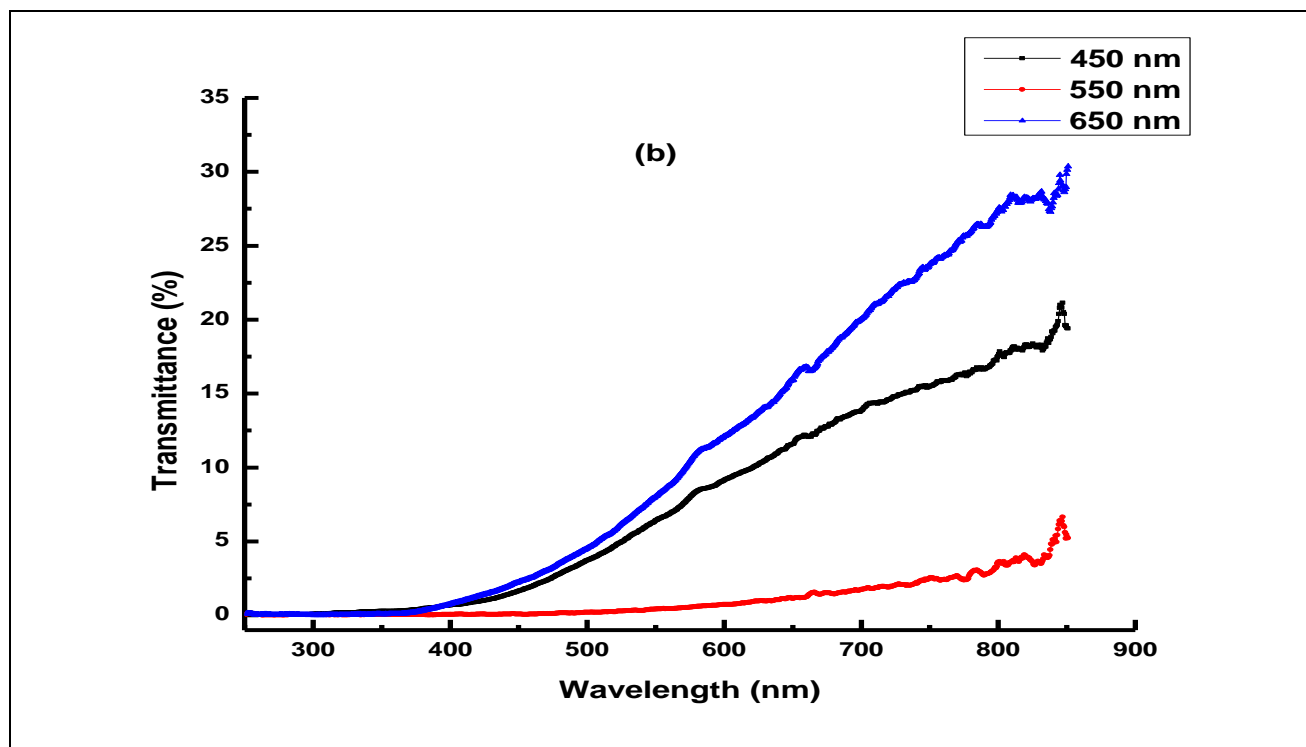
Figure 5b: Optical Transmittance of as-deposited CZTS samples
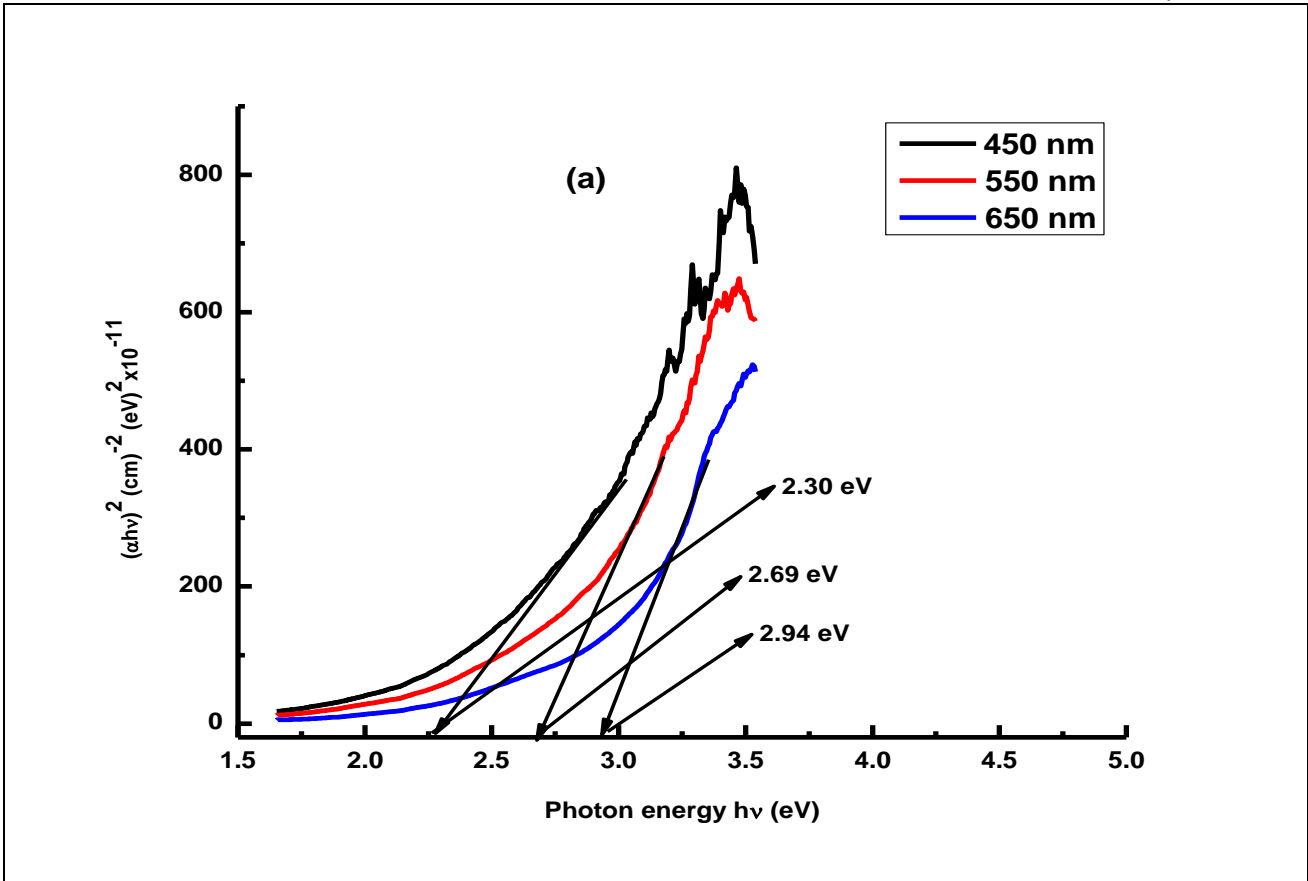
Figure 6a: Optical band gap of as-deposited and annealed
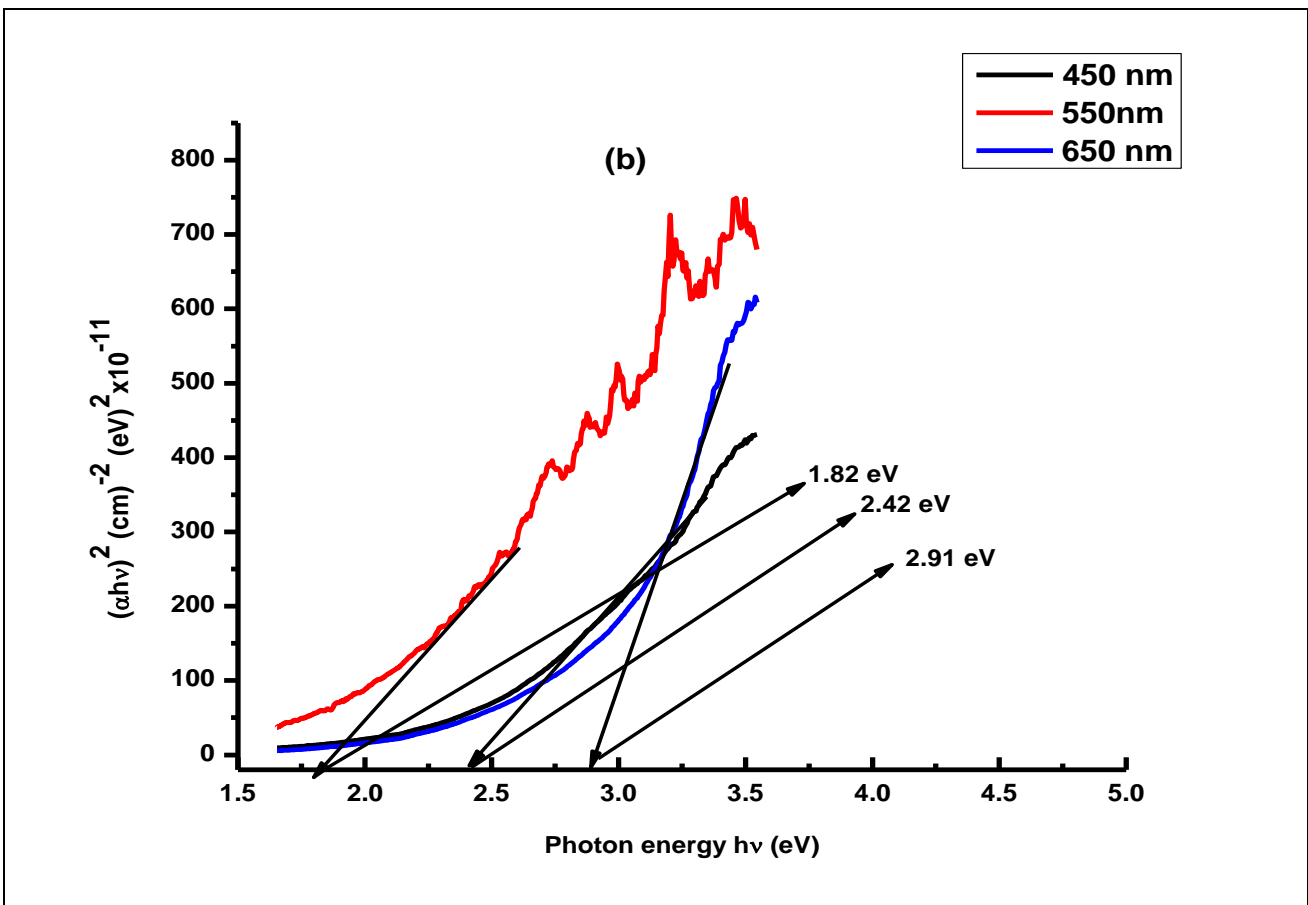
Figure 6b: Optical band gap of as-deposited CZTS samples
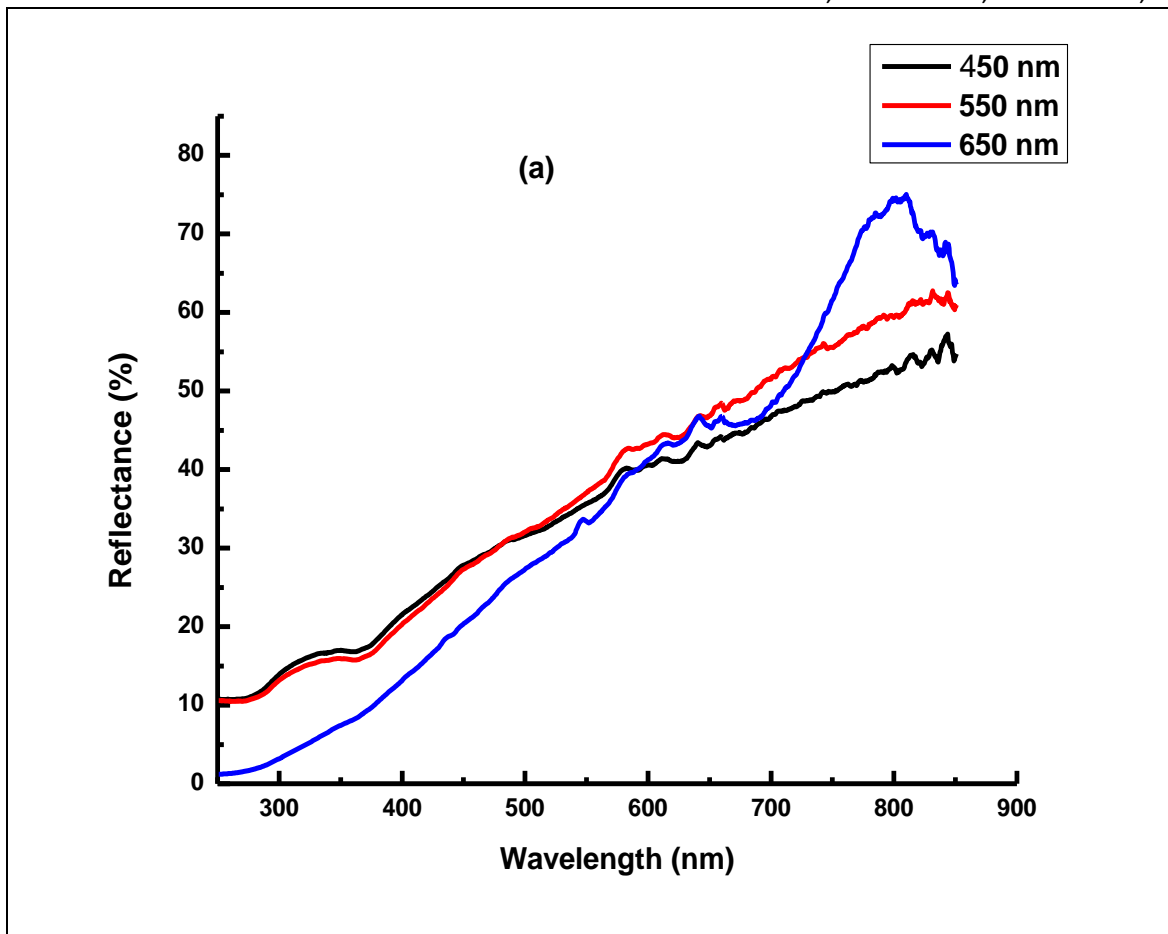
Figure 7a: Optical reflectance of as-deposited and annealed.
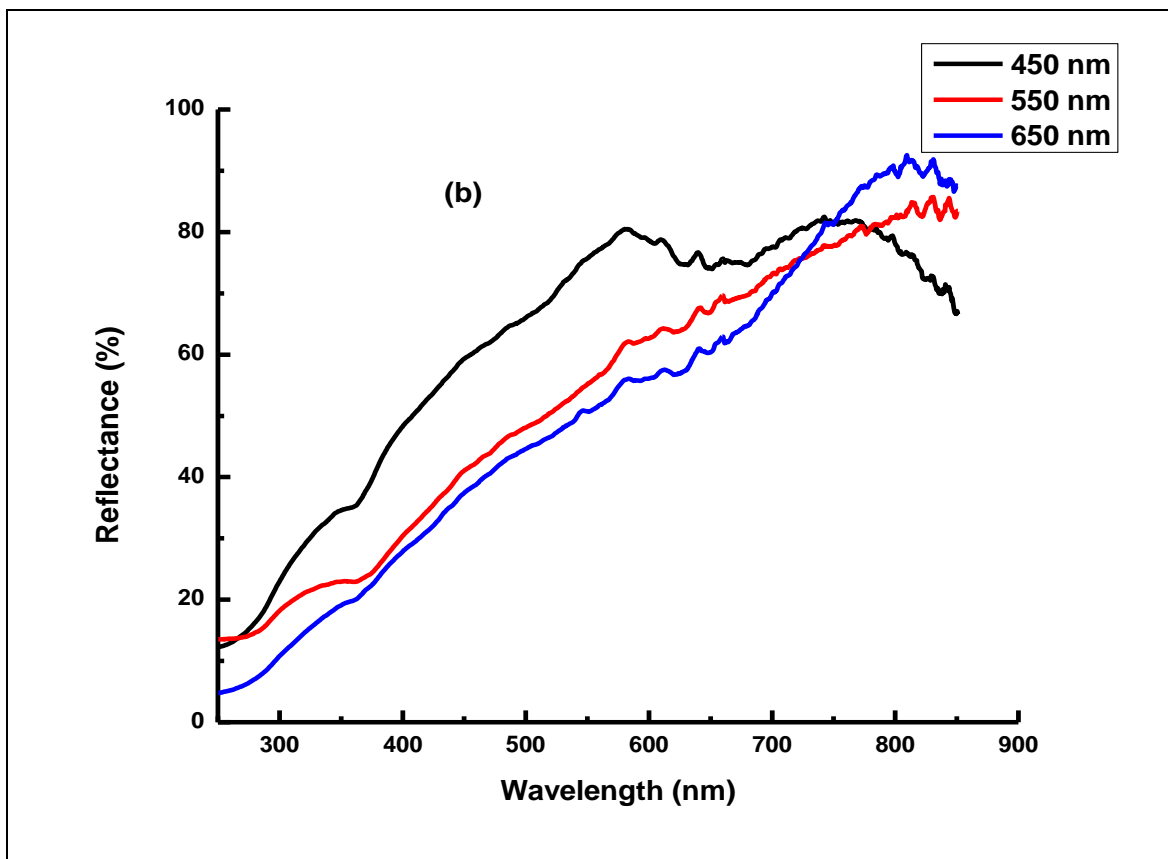
Figure 7b: Optical reflectance of as-deposited CZTS samples.
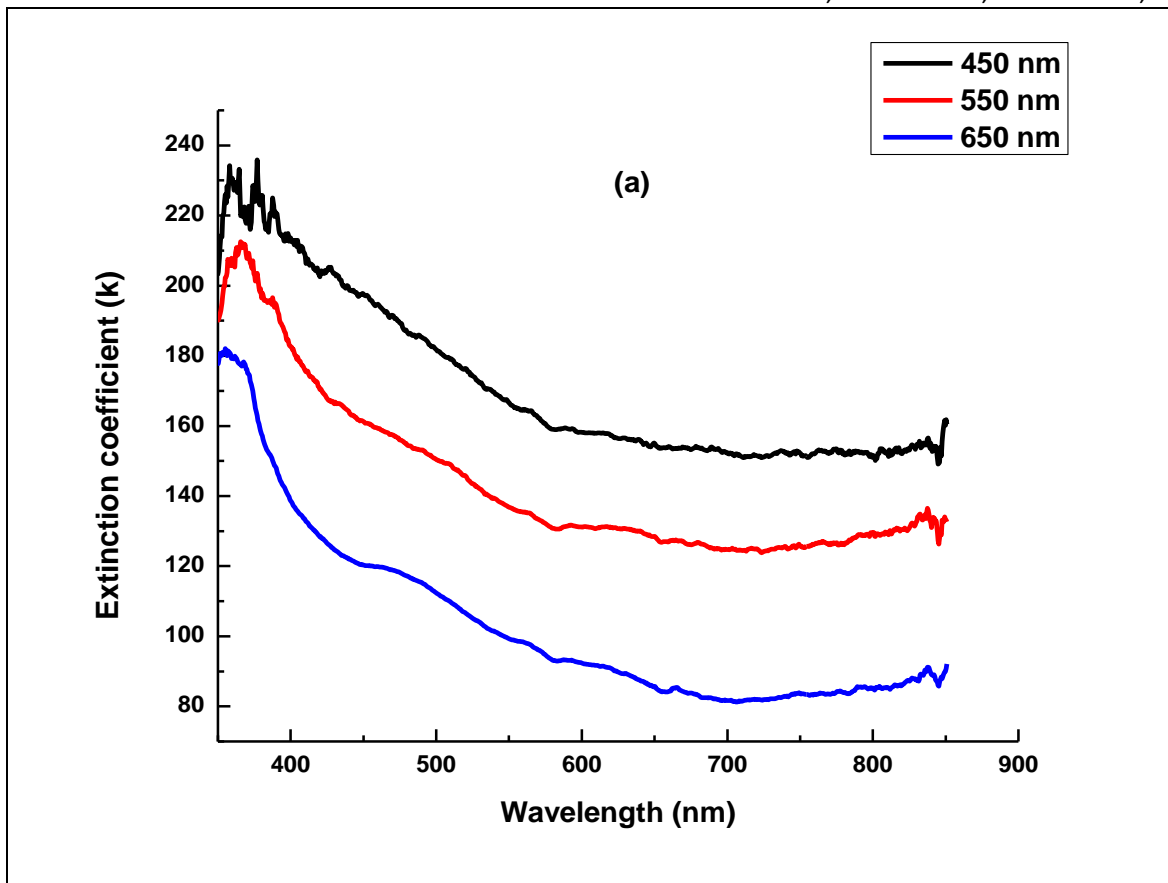
Figure 8a: Extinction coefficient of as-deposited and annealed
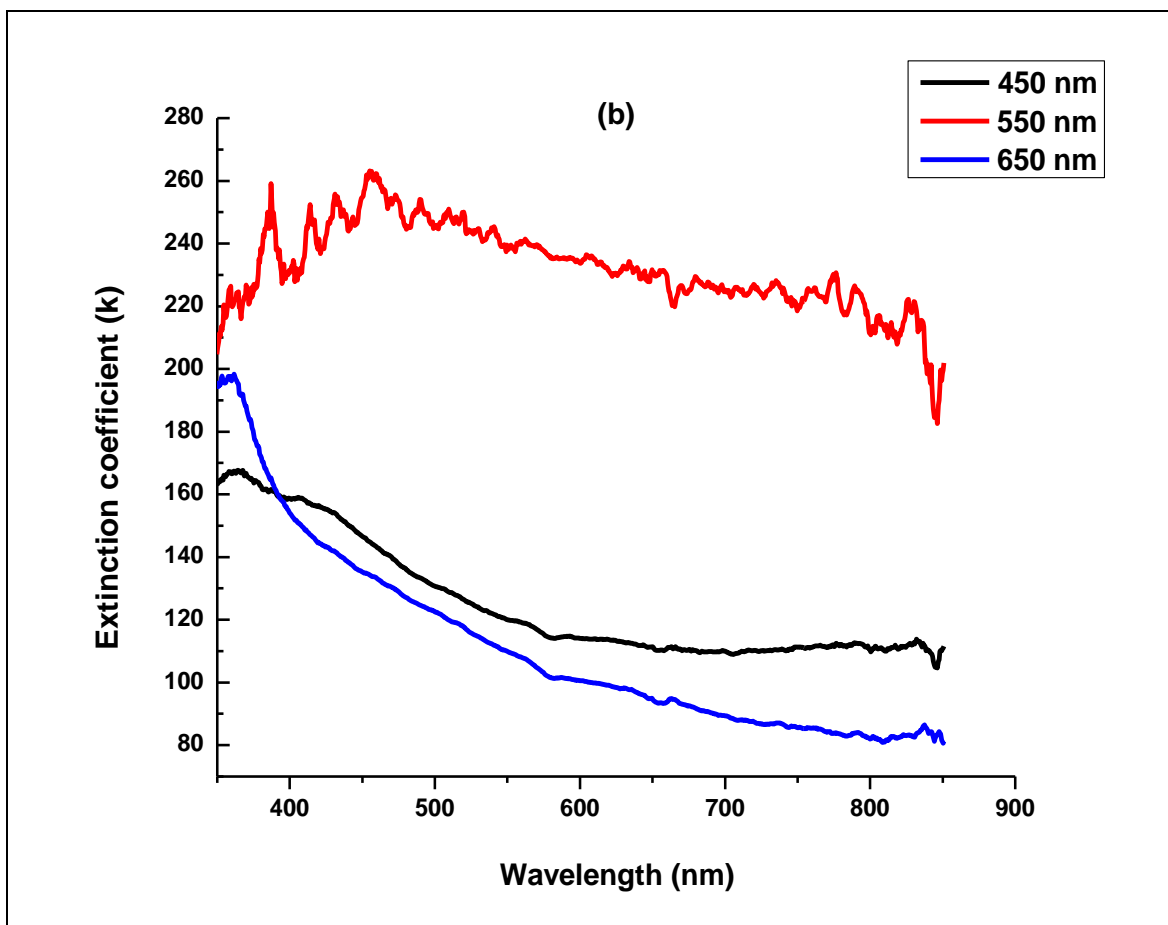
Figure 8b: Extinction coefficient of as-deposited CZTS samples
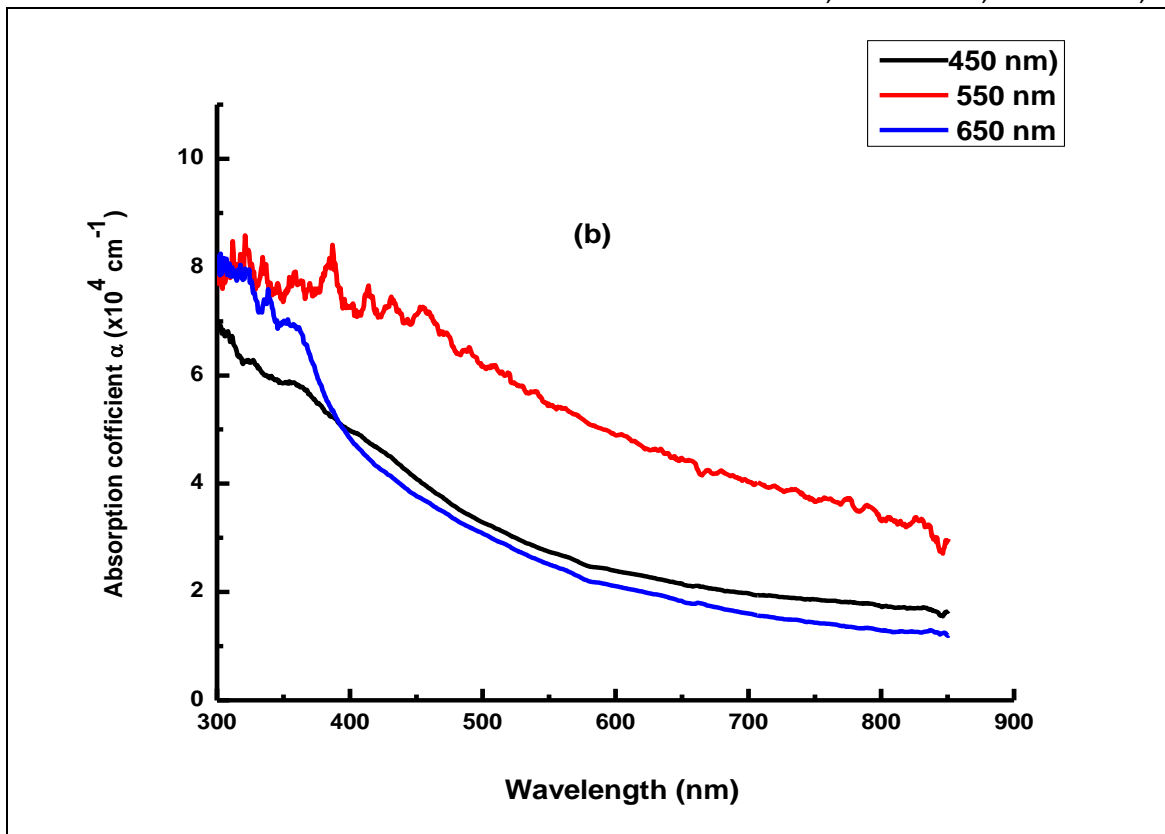
Figure 9a: Absorption coefficient of as-deposited and annealed
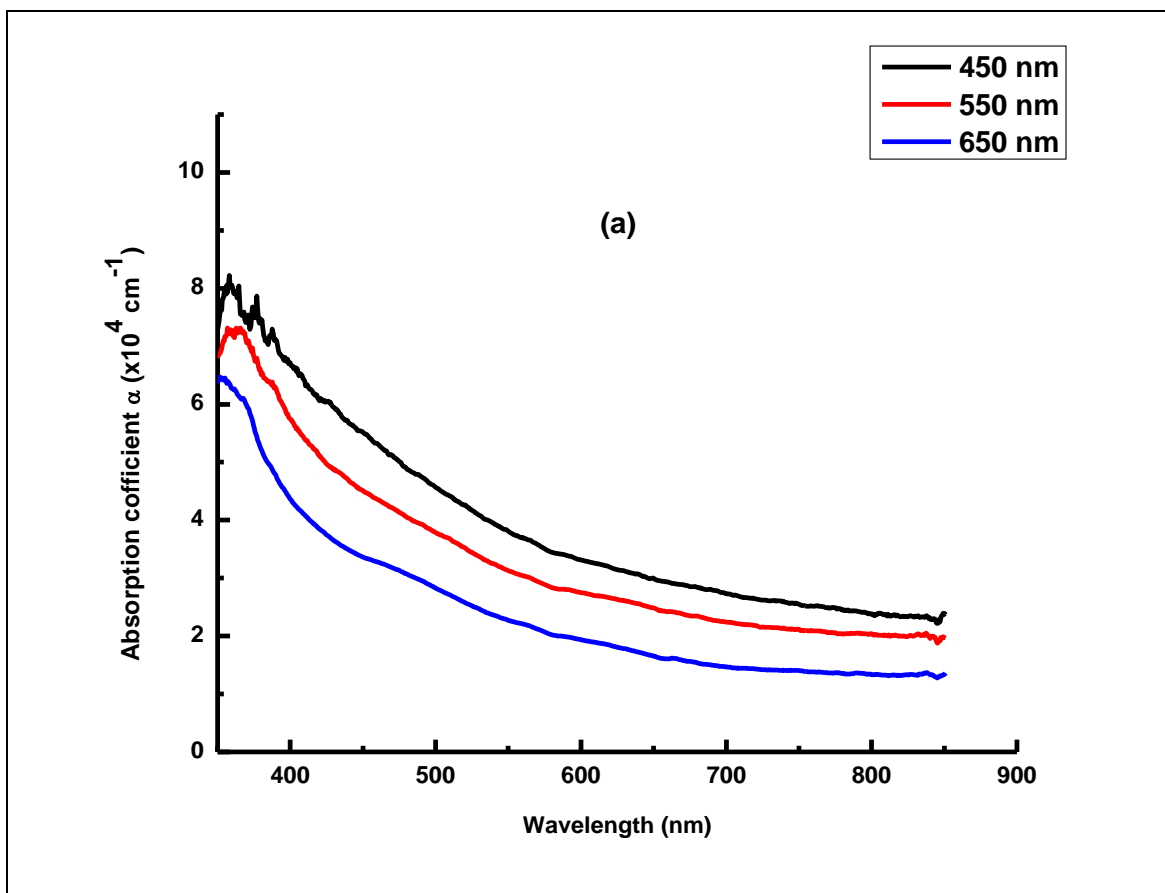
Figure 9b: Absorption coefficient of as-deposited CZTS samples

Figures 10 (a) and 10 (b) show the refractive index (n) versus wavelength, which represents how much light is

bent or **refracted** when it enters the CZTS thin films. It is a critical optical property that characterizes how light

interacts with the material. This parameter can be determined from Equation [4] by (Zhou et al., 2013).

$$n_r = \frac{1+\sqrt{R}}{1-\sqrt{R}} \qquad (4)$$

It is clear that n_r varies for the as-deposited samples. For the annealed samples, n_r decreases with an increase in thickness and the wavelength in the range of 300–800 nm.

There might be more voids in the samples, which would explain the drop in the refractive index (n_r). It is noteworthy that the density of voids is the primary factor influencing n_r. The annealing process appears to enhance n_r, suggesting that n_r of CZTS thin films can be adjusted.

Table 3 summarises the Urbach Energy (E_u) Refractive index, Resistivity, and Sheet resistance of the CZTS thin films.

Gupta et al. (2023) stated that a sample's metal ratio may also be the cause of a change in resistivity. It is possible that the band gap region's shallow states, which cause the production of donors and acceptors and ultimately self-compensation, are the cause of the high resistivity. (AlKhalifah et al., 2020) reported that the decrease in crystal defects may be the cause of the resistivity decrease seen in certain samples. The reported resistivities are consistent with the results of (Zhang et al., 2022). The sheet resistance increases with film thickness for the as-deposited samples. The degree of crystallization may be responsible for this. According to (Ahmadi et al., 2022), the presence of ternary phases may be responsible for the variation in the resistivity of the samples

The Urbach energy (E_u) characterizes the extent of disorder in a material as well as provides insights into the electronic structure and optical properties. Generally, higher Urbach energy indicates more disorder or defects in the material. Furthermore, E_u plays a vital part in the process of discovering solutions to band tailing problems associated with structural disorder, phonons, excitons, and contaminants. Urbach's tail refers to the absorption edge that is below the energy gap, which rises exponentially. The Urbach energy is explained within the context of Einstein's model, and it is possible to condense it into an empirical formula represented in Equation [5] by (Ganshuk et al., 2020).

$$\alpha = \alpha_0 \exp\left(\frac{hv}{E_u}\right) \qquad (5)$$

where α_0 is a constant, E_u denotes an energy which is fixed and interpreted as the width of the tail of localized states in the band gap. The Urbach energy E_u can be estimated from the slope of the straight line of plotting ln(α) versus incident photon energy, hv

The Urbach energies of the as-deposited and the annealed samples of CZTS thin films were determined from Figures 11 (a) and 11 (b). In both Figures, Ln (α) increases with an increase in the photon energy, which suggests that the absorption coefficient increases nonlinearly with increasing photon energy. This might suggest a regime where higher energy photons are more readily absorbed. It is observed from Figure 11 (a) that Ln (α) increases with an increase in energy. This pattern has also been observed for the annealed samples.

The variation in EU values with the increase in film thickness could be attributed to the increase in film disorder, which deepens the band tail that extends in the gap (Sultana et al., 2022). Variation in E_u can also be attributed to the more rigid molecular geometry and the compact intermolecular packing (Sanchez et al., 2016).
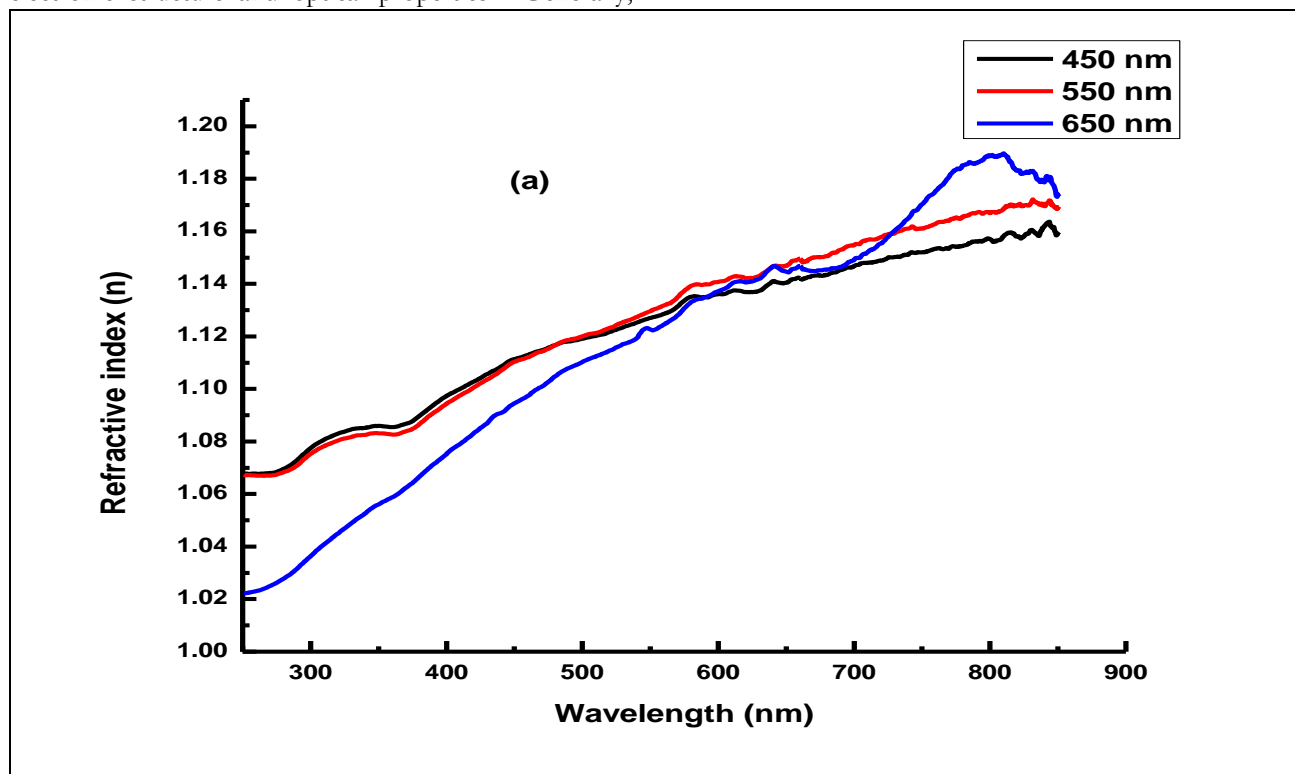
Figure 10a: Refractive index of as-deposited and annealed
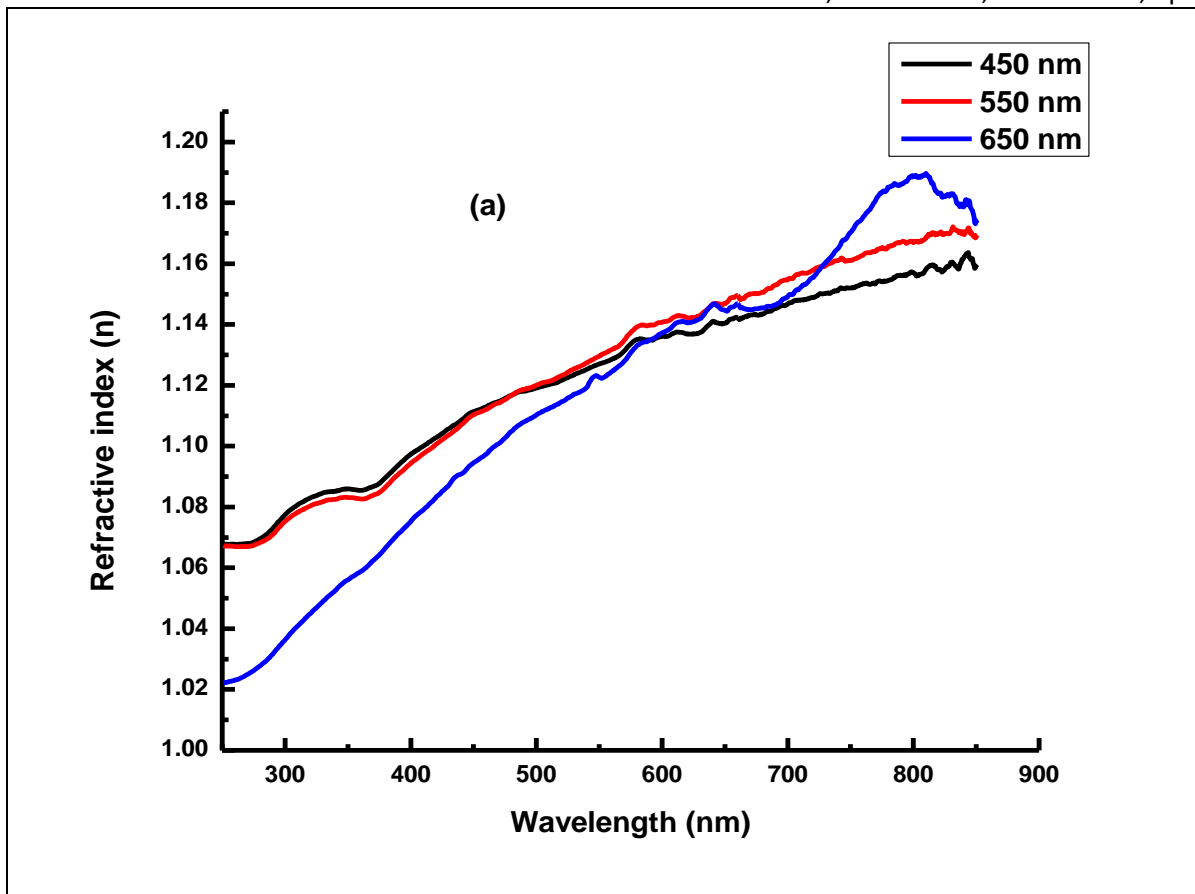
Figure 10b: Refractive index of as-deposited CZTS samples
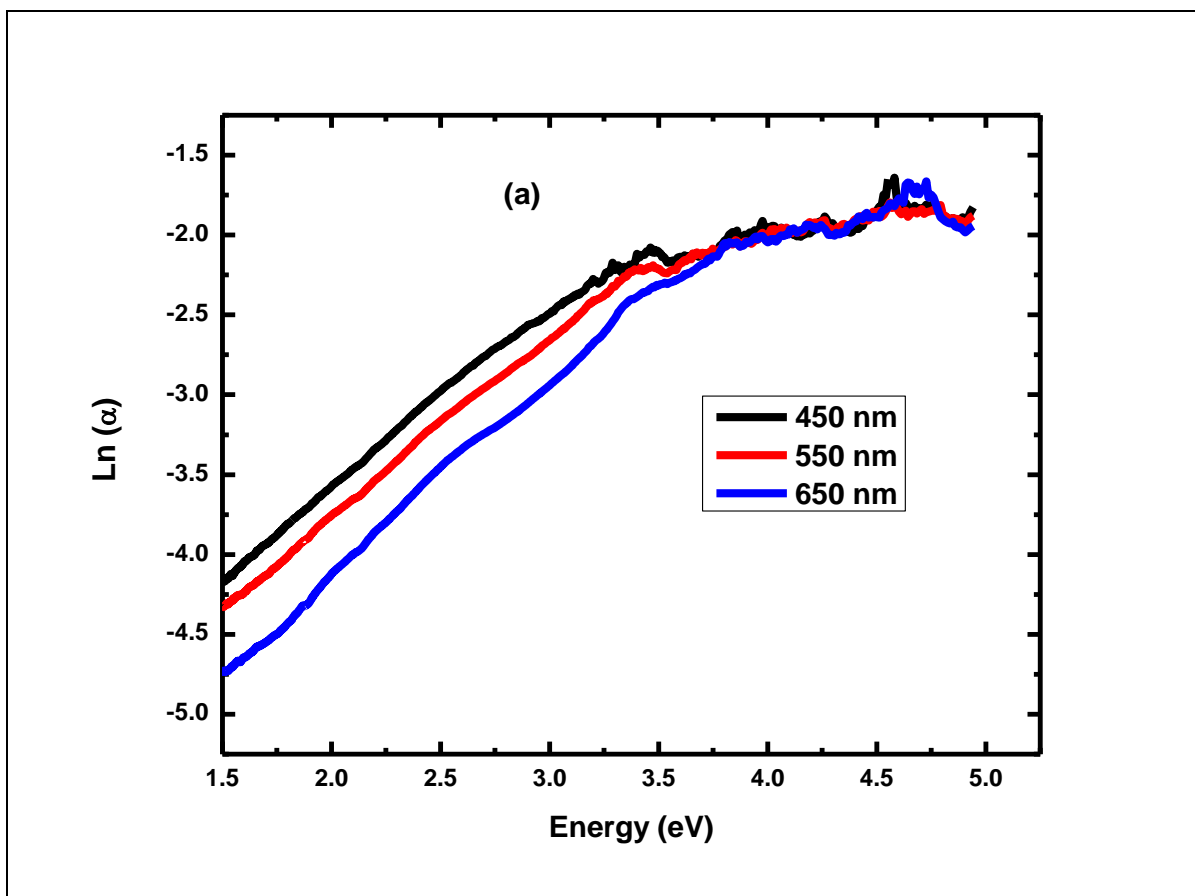
Figure 11a: Ln (α) versus photon energy of as-deposited and annealed
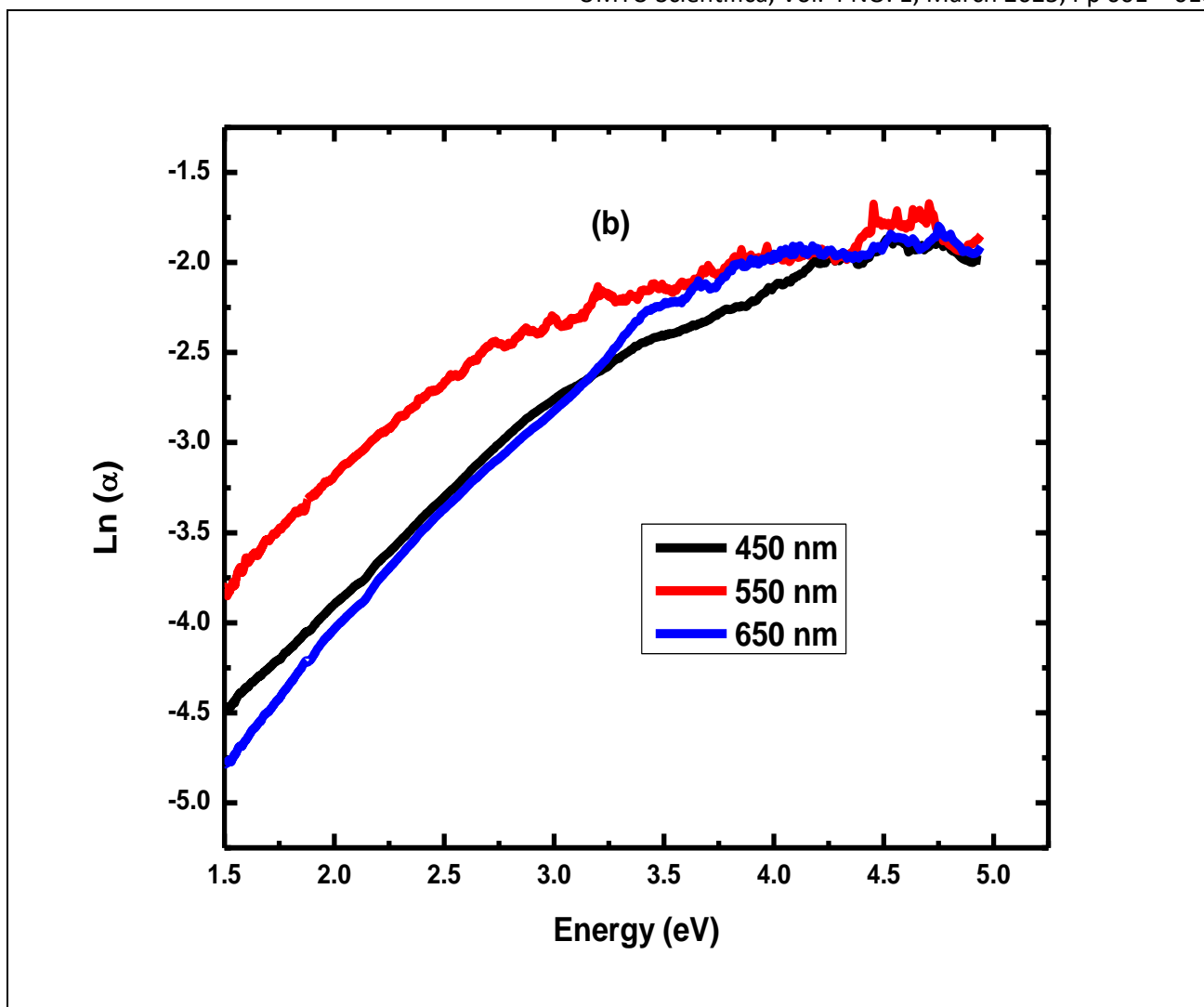
Figure 11b: Ln (α) versus photon energy of as-deposited CZTS samples

Table 3: Urbach energy and refractive index

Sample	Urbach Energy (E_U)	Refractive index (n)	Resistivity (Ω cm)	Sheet Resistance ($\Omega/\square$)
450 nm as-deposited	0.8435	1.12	$4.1 \times 10^{-3}\Omega$ cm	$0.02 \times 10^3\Omega/\square$
550 nm as-deposited	0.8823	1.12	$6.0 \times 10^{-3}\Omega$ cm	$0.03 \times 10^3\Omega/\square$
650 nm as-deposited	0.7989	1.11	$1.4 \times 10^{-3}\Omega$ cm	$0.07 \times 10^3\Omega/\square$
450 nm annealed	0.8442	1.16	$14680 \times 10^{-3}\Omega$ cm	$0.25 \times 10^3\Omega/\square$
550 nm annealed	0.9018	1.15	$35320 \times 10^{-3}\Omega$ cm	$0.15 \times 10^3\Omega/\square$
650 nm annealed	0.7705	1.14	$280 \times 10^{-3}\Omega$ cm	$0.015 \times 10^3\Omega/\square$

CONCLUSION

In conclusion, the deposition of thin films of copper zinc tin sulphide (CZTS) on uncoated soda lime glass substrates has been successfully carried out and thoroughly characterized using X-ray diffraction (XRD), Raman spectroscopy, and UV-Vis spectroscopy. The presence of kesterite CZTS and secondary phases such as SnS (TS), ZnS, and CuSnS (CTS) in the grown thin films has been identified, providing valuable insights into their crystalline structure. The UV-Vis spectroscopy results indicate that some of the samples exhibit high transmittance (>90%) in the visible region, highlighting their potential for transparent and efficient electronic and optoelectronic applications. Additionally, the study of the effect of thickness and annealing temperature on the optical energy gap (Eg) revealed a range of values, with the annealed samples exhibiting narrower energy gaps compared to the as-deposited ones. These findings contribute to our understanding of CZTS thin film properties and offer important considerations for optimizing their performance in various applications.

CRediT Authorship Contribution Statement

Sanusi Abdullahi: Conceptualization, Data curation, Funding acquisition, **Musa Momoh**: Writing – original

draft review and editing, Validation, **Abubakar Umar Moreh**: Supervision, Project administration, Investigation, Resources and **Muhammad Aliyu Wara:** Research Assistant.

DECLARATION OF COMPETING INTEREST

The authors declare that they have no known competing interests that could have appeared to influence the work reported in this communication.

ACKNOWLEDGMENTS

REFERENCES

Abdullahi. S., M. Momoh, A. U. Moreh, A. M. Bayawa and A. saidu (2020). Synthesis and characterization of CZTS thin films from compound target deposited by RF sputtering method. IOP conf. Series Mater. Sci. Eng. 805. ISSN 1757-8981. **[Crossref]**

Ahmad, R., Saddiqi, N., Wu, M., Prato, M., Spiecker, E., Wolfgang Peukert, W and Distaso, M (2021). Phase evolution of Cu_2ZnSnS_4 (CZTS) nanoparticles from *in situ* formed binary sulphides under solvothermal conditions. *Cryst. Eng .Comm*, 2021, 23, 7944-7954. **[Crossref]**

Ahmadi, S., Khemiri, N., Cantarero, A., & Kanzari, M. (2022). XPS analysis and structural characterization of CZTS thin films deposited by one-step thermal evaporation. *Journal of Alloys and Compounds*, *925*, 166520, ISSN 0925-8388, Elsevier BV, **[Crossref]**

Ahmed, Z., Bouchaib, H., Hicham, L., Youssef, D., HervÈ JoÎl Tchognia, N., Youssef, N., Salah, F., Abdelkrim, B., Mounia, T., Abderraouf, R and Philippe, T (2022). Investigation of CZTS absorber layer deposited by spin coating technique for photovoltaic applications. *Materials Today: Proceedings*, *53*, 355-360, ISSN 2214-7853, Elsevier BV. **[Crossref]**

Aksoy, S., Caglar, Y., Ilican, S., Caglar, M (2009). Effect of heat treatment on physical properties of CdO films deposited by sol-gel method. International Journal of Hydrogen Energy, 34 (12), 5191-5195. **[Crossref]**

Alkhalifah, M., El Radaf, I.M., & El-Bana, M.S. (2020). New window layer of $Cu_2CdSn_3S_8$ for thin film solar cells. Journal of Alloys and Compounds, 813, 152169. **[Crossref]**

El Radaf, I. M (2020). Dispersion parameters, linear and nonlinear optical analysis of the $SnSb_2S_4$ thin films. Applied Physics A (2020) 126:357, 1-10. **[Crossref]**

Al-Zahrani, H. Y. S (2020). Synthesis, optical and optoelectrical analysis of the Cu_2CoSnS_4 thin

films as an absorber layer for thin-film solar cells. Journal of Materials Science: Materials in Electronics. **[Crossref]**

Balaji, G., Prabavathy, N., Balasundaraprabhu, R., Prasanna, S., Echeverria, E., McIlroy, D. N., Sivakumaran, K., Kannan, M. D., Velauthapillai, D (2020). Investigations on post sulphurised Cu_2ZnSnS_4 absorber layer thin films prepared using radio frequency magnetron sputtering, Thin Solid Films, Volume 695, **[Crossref]**.

Barragan, A. A., Malekpour, H., Exarhos, S., Balandin, A. A and Mangolini, L (2016). Grain-to-grain compositional variations and phase segregation in CZTS films ACS Appl. Mater. Interfaces, Just Accepted Manuscript

Behera, N and Mohan, B (2019). The phase optimization, optical and electrical properties of kesterite Cu_2ZnSnS_4thin film prepared by single target RF magnetron sputtering technique for solar cell application. *Mater. Res. Express* 6126457. **[Crossref]**

Chander, S., Tripathi, S. K., Kaur, I and Arijit, K. De (2024). Non-toxic and earth-abundant Cu2ZnSnS4 (CZTS) thin film solar cells: A review on high throughput processed methods, *Materials Today Sustainability,* 25, 100662. **[Crossref]**

Demir, K.C (2021). The investigation of the corrosion behaviour of CZTS thin films prepared via electrodeposition. *Materials Science in Semiconductor Processing*, Elsevier. **[Crossref]**

Diwate, K., Mohite, K., Shinde, M., Rondiya, S., Pawbake, A., Date, A., Pathan, H and Jadkar, S. (2017). Synthesis and Characterization of Chemical Spray Pyrolysed CZTS Thin Films for Solar Cell Applications. *Energy Procedia.* 110. 180-187. **[Crossref]**

Dong, M., Wei, L and Zhu, Y (2023). Controllability study of copper-tin-sulphide (Cu_3SnS_4) material based on the ratio adjustment of Cu to Sn elements. *Micro & Nano Letters* 18 (9-12) e12176. **[Crossref]**

El Mahboub, E., El Khouja, O., Bocirnea, A. E., Zakaria, S., Galca, A. C., Mansori, M and Hichou, A (2024). Investigation of kesterite to stannite phase transition and band gap engineering in Cu2Zn1-xCoxSnS4 thin films prepared by sol-gel spin coating, *Applied Surface Science*, 672. **[Crossref]**

Ezealigo, B. N., Nwanya, A. C., Simo, A., Osuji, R.U., Bucher, R., Maaza, M and Ezema, F. I. (2017). Optical and electrochemical capacitive properties of copper (I) Iodide thin film deposited by SILAR method. *Arabian Journal of Chemistry.* **[Crossref]**.

Feng, J., Huang, X., Chen, W., Wu, J., Lin, H., Cheng, Q and Zhang, F. (2016). Fabrication and characterization of Cu_2ZnSnS_4 thin films for photovoltaic application by low-cost single target sputtering process. *Vacuum*, **126** 84–90.

[Crossref]

Gadallah, A.-S., Salim, M. A., Atwee, T., & Ghander, A. M. (2018). Effect of Al doping on structural, morphological, optical, and electrical properties of Cu₂ZnSnS₄ thin films prepared by sol-gel spin coating. *Optik, 159,* 275–282. **[Crossref]**

Gansukh, M., López Mariño, S., Espindola Rodriguez, M., Engberg, S. L. J., Martinho, F. M. A., Hajijafarassar, A., and Canulescu, S. (2020). Oxide route for production of Cu₂ZnSnS₄ solar cells by pulsed laser deposition. *Solar Energy Materials and Solar Cells, 215,* 110605. **[Crossref]**

Gezgin, Y., Houimi, A., Mercimek, B and Kiliç, H. S (2020). The Effect of CZTS Ultrathin Film Thickness on the Electrical Characteristic of CZTS/Si Heterojunction Solar Cells in the Darkness and under the Illumination Conditions. Silicon, 1-13. **[Crossref]**

Gupta, A. S. K., Farhad, S. F. U., Habib, M. S., Hossan, M. R., Hossain, K., Das, N. K., Quamruzzaman, M., Matin, M. and Amin, N (2023). Characterizations of extrinsically doped CZTS thin films for solar cell absorbers fabricated by sol-gel spin coating method. Applied Surface Science Advances. 13, 1-12. **[Crossref]**.

Hameed, S. A., Bakr, N. A., Hassan, A. M and Jasim, A. M (2020). Structural and Optical Properties of Cu₂ZnSnS₄ Thin Films Fabricated by Chemical Spray. AIP Conference Proceedings 2213, 020082; **[Crossref]**

Hassanien, A. S and Akl, A. A (2019). Optical characterizations and refractive index dispersion parameters of annealed TiO₂ thin films synthesized by RF-sputtering 2 technique at different flow rates of the reactive oxygen gas, *Physica B: Physics of Condensed Matter*, **[Crossref]**

Islam, M. A., Aziz, A., Witjaksono, G and Amin, N. (2013). Structural, Electrical and Optical Properties of Zn Rich CZTS Thin Film, 90–93. Unpublished. 23-30. **[Crossref]**

Jagdish, P., Jagavendra, Y., Sunil, K., Hansraj, S and Mangej, S (2023). Impact of Sb Incorporation on the Structural and Optical Properties of CZTS Thin Films Grown by Spin Coating Technique. *Oriental Journal Of Chemistry*, 39(3), 596-603, ISSN 2231-5039, Oriental Scientific Publishing Company. **[Crossref]**

Khushaim, M., Alamri, S., Kattan, N., Jaber, A and Alamri, S (2021). Study of kesterite Cu₂ZnSnS₄ (CZTS) thin films deposited by spray technique for photovoltaic applications, *Journal of Taibah University for Science*, 15:1, 329-339, **[Crossref]**

Kwak, J. I., Nam, S. H., Kim, L., & An, Y. J. (2020). Potential environmental risk of solar cells: Current knowledge and future challenges. Journal of Hazardous Materials, 392, 122297. ISSN 0304-3894. **[Crossref]**

Ma, C., Lu, X., Xu, B., Zhao, F., An, X., Li, B, Sun, L., Jiang, J., Chen, Y and Chu, J. (2019). Effects of sputtering parameters on photoelectric properties of AZO film for CZTS solar cell. *Journal of Alloys and Compounds*, *774*, 201-2. doi: **[Crossref]**

Maheshwari, B. U., & Kumar, V. S. (2015). Phase transformation of solution-based p-type Cu₂ZnSnS₄ thin film: applicable for solar cell. *International Journal of Energy Research*, *39*(6), 771-777. **[Crossref]**

Moon, Md. M. A., Rahman, Md. F., Hossain, J., & Ismail, A. B. Md. (2019). Comparative Study of the Second Generation a-Si:H, CdTe, and CIGS Thin-Film Solar Cells. Advanced Materials Research, 1154, 102–111. **[Crossref]**

Munir, B., Prastyo, B. E., Nurjaya, M. N., Muslih, E. Y., and Alfauzan, S. K (2016). High crystalline Cu₂ZnSnS₄ semiconductor prepared from low toxicity ethanol-based precursors. International Conference on Engineering, Science and Nanotechnology 2 1788, 030022 (2017). **[Crossref]**

Olalekan C. Olatunde, Damian C. Onwudiwe, (2021). Stoichiometric phases and mechanism of crystal phase selectivity of copper-based ternary sulphides. *Materials Science in Semiconductor Processing,*125. **[Crossref]**.

Olgar, M. A., A. Seyhan., A. O. Sarp., and R. Zan (2020). Impact of sulfurization parameters on properties of CZTS thin films grown using quaternary target. J Mater Sci: Mater Electron, **[Crossref]**

Orletskyi, M.M., Solovan, V.V., Brus, F., Pinna, G., Cicero, P.D., Maryanchuk, E.V., Maistruk, M.I., Ilashchuk, T.I., Boichuk and Tresso, E (2016). Structural, optical and electrical properties of Cu2ZnSnS4 films prepared from a non-toxic DMSO-based sol-gel and synthesized in low vacuum, Journal of Physical and Chemistry of Solids, **[Crossref]**

Park, J., Yoo, H., Karade, V., Gour, K. S., Choi, E., Kim, M Hao, X., Shin, S. J., Kim, J., Shim, H., Kim, D., Kim, J. H., Yun, J and Kim, J. H (2020). Investigation of low-intensity light performances of kesterite CZTSe, CZTSSe, and CZTS thin film solar cells for indoor applications. J. Mater. Chem. A, 1-7. **[Crossref]**

Paul, R., Shukla, S., Lenka, T.R. (2024). Recent progress in CZTS (CuZnSn sulfide) thin-film solar cells: a review. *J Mater Sci: Mater Electron* **35**, 226. **[Crossref]**

Prabeesh, P., Sajeesh, V. G., Selvam, I. P., Bharati, M. D., Rao, G. M., and Potty, S. N. (2020). CZTS solar cell with non-toxic buffer layer: A study on the sulphurization temperature and absorber layer thickness. *Solar Energy*, *207*, 419-427. **[Crossref]**

Rabeh, M., Ben, T. R and Kanzari, M. (2013). Substrate Temperature Effects on Structural Optical and Electrical Properties of Vacuum Evaporated Cu₂ZnSnS₄ Thin Films. *International Journal of Engineering Practical Research*, *2* (2), 71–76.

Rahman, M. A and Khan, M. K. R (2014). Effect of annealing temperature on structural, electrical

and optical properties of spray pyrolytic nanocrystalline CdO thin films. *Materials Science in Semiconductor Processing* 24, 26–33. **[Crossref]**https://doi.org/10.1016/j.mssp.2014.03.002

Sadanand, S., Lohia, P and Dwivedi, D. K (2020). Contribution to sustainable and environmental friendly non-toxic CZTS solar cell with an innovative hybrid buffer layer, *Solar Energy,* 204, 748-760. **[Crossref]**.

Saiful Islam, M., Doroody, C., Kiong, T. S., Za abar, F. I., Bahrudin, M., Rahman, K. S., Kar, Y. B and Zuhdi, A. W. M (2024). A comprehensive modeling on MoS2 interface and defect engineering in CZTS thin film solar cells. *Journal of Materials Research and Technology.* 33, 6601-6609. **[Crossref]**

Salunkhe, R. R., Dhawale D. S., Gujar, T. P., Lokhande, C. D (2009). Structural, electrical and optical studies of SILAR deposited cadmium oxide thin films: Annealing effect. Materials Research Bulletin, 44 (2), 364-368, **[Crossref]**

Sanchez, T. G., Mathew, X., and Mathews, N. R. (2016). Obtaining phase-pure CZTS thin films by annealing vacuum evaporated CuS/ZnS stack. *Journal of Crystal Growth*, **445**, 15-23. **[Crossref]**

Stamford, L and Azapagic, A (2019). Environmental impacts of copper-indium-gallium-selenide (CIGS) photovoltaics and the elimination of cadmium through atomic layer deposition, *Science of The Total Environment*, 688, 1092-1101. **[Crossref]**.

Sultana, M., Siddika, A., Mahmood, S. S., Sharmin, A., Tabassum, S., Rahman, M., and Bashar, M. S (2022). Fabrication of CZTS thin films by ultrasonic spray pyrolysis at a low substrate temperature and effect of tin concentration on the characteristics of the CZTS thin films. *Bangladesh Journal of Scientific and Industrial Research*, *57*(1), 1-6, ISSN 2224-7157, Bangladesh Journals Online (JOL), **[Crossref]**

Yang, Y., Ding, Y., Zhang, J., Liang, N., Long, L., and Liu, J (2022). Insight into the Growth Mechanism of Mixed Phase CZTS and the Photocatalytic Performance. *Nanomaterials*, 12, 1439. **[Crossref]**

Yeh, Min-Yen., Po-Hsun Lei., shao-Hsein and Chyi-da, Yang (2016). Copper-Zinc-Tin-Sulfur Thin Film Using Spin-Coating Technology. *Materials.* 9 (526), 1-12. **[Crossref]**

Zhang, C., Mahadevan, S., Yuan, J., Ho, J. K. W., Gao, Y., Liu, W., ... & So, S. K. (2022). Unraveling Urbach tail effects in high-performance organic photovoltaics: dynamic vs static disorder. *ACS Energy Letters*, *7*(6), 1971-1979. **[Crossref]**

Zhou, S., Tan, R., Jiang, X., Shen, X., Xu, W., and Song, W. (2013). Growth of CZTS thin films by sulfurization of sputtered single-layered Cu-Zn-Sn metallic precursors from an alloy target. *Journal of Materials Science: Materials in Electronics*, **24** (12), 4958–4963. **[Crossref]**

Ziti, A., Hartiti, B., Labrim, H., Fadili, S., Ridah, A., Belhorma, B., Tahri, M. & Thevenin, P. (2018). Study of kesterite CZTS thin films deposited by spin coating technique for photovoltaic applications. *Superlattices and Microstructures*, *127*, 191-200. **[Crossref]**